TU Delft

Delft University of Technology

Techno-economic assessment of off-grid hydrogen supply from distant solar or wind sources to steelmaking

Li, Longquan; Aravind, Purushothaman Vellayani; Boldrini, Annika; van den Broek, Machteld

DOI
10.1016/j.apenergy.2025.125947

Publication date
2025

Document Version
Final published version

Published in
Applied Energy

Citation (APA)
Li, L., Aravind, P. V., Boldrini, A., & van den Broek, M. (2025). Techno-economic assessment of off-grid hydrogen supply from distant solar or wind sources to steelmaking. *Applied Energy*, *391*, Article 125947. https://doi.org/10.1016/j.apenergy.2025.125947

Important note
To cite this publication, please use the final published version (if applicable).
Please check the document version above.

Copyright
Other than for strictly personal use, it is not permitted to download, forward or distribute the text or part of it, without the consent of the author(s) and/or copyright holder(s), unless the work is under an open content license such as Creative Commons.

Takedown policy
Please contact us and provide details if you believe this document breaches copyrights.
We will remove access to the work immediately and investigate your claim.

This work is downloaded from Delft University of Technology.
For technical reasons the number of authors shown on this cover page is limited to a maximum of 10.

Applied Energy 391 (2025) 125947

Contents lists available at ScienceDirect

Applied Energy

journal homepage: www.elsevier.com/locate/apenergy

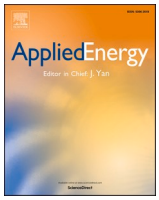

Techno-economic assessment of off-grid hydrogen supply from distant solar or wind sources to steelmaking

Longquan Li [a,*], Purushothaman Vellayani Aravind [a], Annika Boldrini [b,c], Machteld van den Broek [d]

[a] Energy and Sustainability Research Institute Groningen, University of Groningen, 9747, AG, Groningen, the Netherlands.
[b] Joint Research Centre, European Commission, Westerduinweg 3, 1755, LE, Petten, the Netherlands
[c] Copernicus Institute of Sustainable Development, Utrecht University, Princetonlaan 8a, 3584, CB, Utrecht, the Netherlands
[d] Faculty Technology, Policy, and Management, Delft University of Technology, Jaffalaan 5, 2628 BX, Delft, PO Box 5015, 2600, GA, the Netherlands

HIGHLIGHTS

- Techno-economic evaluation of 61 off-grid hydrogen supply chains for steelmaking.
- Compressed hydrogen chains with underground storage have the lowest cost.
- Liquid organic hydrogen carrier chains have the second lowest cost.
- Methanol- or ammonia-based chains are not cost-effective due to low efficiency.
- Storage should be near demand in liquid hydrogen chains but near supply in other chains.

ARTICLE INFO

Keywords:
Hydrogen supply chain
Techno-economic assessment
Hydrogen-based direct reduced iron

ABSTRACT

Off-grid hydrogen supply from solar or wind sources to hydrogen-based steelmaking can reduce CO_2 emissions. However, the techno-economic feasibility of different supply chain configurations remains uncertain. This study evaluates 61 off-grid hydrogen supply chains for a 15 Mt. steel/year plant in 2030, considering renewable energy sources (onshore/offshore wind, solar, and overseas options), transmission technologies (cables, pipelines, trucks, and ships), storage technologies (compressed gaseous hydrogen, liquid hydrogen, ammonia, methanol, and liquid organic hydrogen carriers), and seasonal storage locations (at the energy source or steelmaking plant). Onshore truck transmission of hydrogen is found to be unpromising due to the significantly higher cost compared to alternative transmission technologies. When the transmission technology is not truck, chains with underground compressed hydrogen storage achieve the lowest levelized cost of hydrogen (LCOH) at 3.8–5.6 $€_{2020}$/kg H_2, outperforming other options. When underground hydrogen storage is not feasible, liquid organic hydrogen carriers present the next lowest cost. Chains utilizing ammonia, methanol, and liquid hydrogen exhibit lower efficiency, higher renewables capacity requirement, and consequently higher LCOH, making them less attractive. Electricity transmission lowers the LCOH of compressed hydrogen chains compared to hydrogen pipeline transmission, but for other chains the trend is reversed. Hydrogen storage near the steelmaking plant reduces costs by enabling the reuse of boil-off hydrogen in liquid hydrogen chains, but for other chains storing hydrogen near the renewable energy source lowers the cost. Impacts of input uncertainties on the LCOH, limitations of this study, and suggestions for future studies are also presented.

1. Introduction

Achieving the Paris climate goals requires deep cuts in CO_2 emissions in all sectors [1,2]. The iron and steel industry is essential in many national economies [2]. However, it is both energy-intensive (20.6 GJ/t crude steel cast) and CO_2-intensive (1.9 t_{CO2}/t crude steel cast). In 2022, the global crude steel production reached 1885 Mt. [3,4]. The transition from the current fossil-based primary steel production to low-emission options is necessary, and many projects focusing on emission

* Corresponding author at: Energy Academy Europe Building, Nijenborgh 6, 9747, AG, Groningen, the Netherlands
E-mail address: longquan.li@rug.nl (L. Li).

https://doi.org/10.1016/j.apenergy.2025.125947
Received 2 February 2024; Received in revised form 23 March 2025; Accepted 14 April 2025
0306-2619/© 2025 The Authors. Published by Elsevier Ltd. This is an open access article under the CC BY license (http://creativecommons.org/licenses/by/4.0/).

Nomenclature

ACAPEX	annuity of the capital expenditures (€$_{2020}$)
base	base plant
c	levelized cost of hydrogen (€$_{2020}$/unit)
c_{WasH}	cost of waste heat (€$_{2020}$/MWh)
c_{ReE}	cost of baseload renewable electricity (€$_{2020}$/MWh)
CAPEX_unit.	averaged unit capital expenditures (€$_{2020}$/unit)
CAPEX	capital expenditures (€$_{2020}$)
cond	conditioning
carrier	carrier production
chem	chemical
D	distance (km)
e	unit energy demand (kWh/kg$_{H2}$)
el	electricity
E	energy demand (kWh)
EL	electrolyzer
ENEX	energy related expenses (€$_{2020}$)
l	loss rate of a process (%)
L	energy loss (kWh)
LR	loss rate of each chain step
m	mass flow rate (kg/h)
M	mass (kg)
n	lifetime (year)
O&M	operation and maintenance costs (€$_{2020}$)
OPEX	annual operational expenditures (€$_{2020}$)
P	power (kW)
q	unit heat demand (kWh/kg$_{H2}$)
Q	heat demand (kWh)
recond	reconditioning
ReE	renewable electricity
store	storage
S	size of the plant (t H_2/d)
t	time (h)
WasH	waste heat

Greek letters

α	scaling factor
β	fixed percentage of the total hydrogen mass entering the seasonal storage
ρ	mass ratio
η	efficiency

Abbreviations

ASU	air separation unit
BF/BOF	blast furnace-basic oxygen furnace
CF	capacity factor
CGH_2	compressed gaseous hydrogen
CH_3OH	methanol
DAC	direct air capture
DRI	direct reduced iron
EAF	electric arc furnace
H_2-DRI	direct reduced iron with hydrogen
HVAC	high-voltage alternative current
HVDC	high-voltage direct current
ISI	iron and steel industry
LH_2	liquified hydrogen
LHV	lower heat value
LOHC	liquid organic hydrogen carrier
NH_3	ammonia
PEM	proton exchange membrane
PV	photovoltaic
RES	renewable energy sources
UHS	underground hydrogen storage
WACC	weighted average cost of capital

reduction technologies have been initiated [5,6]. Of the potential decarbonization options, the direct reduction of iron with hydrogen (H_2-DRI) has attracted much attention recently [2,7–9]. Thirty-nine H_2-DRI projects are expected to operate by 2030, of which twenty-four will be at full scale [10]. The deployment of H_2-DRI will result in a hydrogen demand of 50–60 kg$_{H2}$/t steel [11,12], and developing relevant hydrogen supply infrastructure is challenging. Techno-economic evaluation of hydrogen supply options to steelmaking plants is essential for infrastructure planning and policymaking.

Possible hydrogen sources for H_2-DRI include fossil fuel gasification and water electrolysis powered by off-grid renewable energy sources (RES) or the grid. Hydrogen production via electrolysis does not generate direct carbon emission, whereas fossil fuel gasification is highly carbon-intensive [13]. Vogl et al. [11] assessed the techno-economic performance of hydrogen supply to a DRI-electric arc furnace (EAF) plant from the electrolyzers powered by the electricity grid. Their analysis showed that the emissions from the H_2-DRI-EAF would be equivalent to those from the blast furnace-basic oxygen furnace (BF/BOF) processes (1.9 t$_{CO2}$/t$_{liquid\ steel}$) if the power grid emission intensity reaches 0.53 t$_{CO2}$/MWh. Additionally, at an electricity cost of 40 €$_{2018}$/MWh, the production cost of the H_2-DRI-EAF route is 36 % higher than the BF/BOF route. Elsheikh and Eveloy [14] evaluated the techno-economic performance of hydrogen production from a combination of solar photovoltaic (PV) and grid electricity for an H_2-DRI-EAF plant in a solar-rich area. They found that integrating PV reduces the emission intensity of hydrogen production and steelmaking by approximately 36 % (from 0.89 to 0.57 t$_{CO2}$/t$_{liquid\ steel}$) compared to using the grid electricity alone, while also slightly lowering levelized cost of steel production. Superchi et al. [15] assessed the costs and emission of an H_2-DRI-EAF plant using hydrogen produced from a mix of grid electricity and wind energy in Italy. They found that the emission intensity of the H_2-DRI-EAF process under the most cost-effective configuration is approximately 0.33 t$_{CO2}$/t$_{liquid\ steel}$, with a levelized cost of hydrogen at 5.7 €$_{2022}$/kg$_{H2}$.

To avoid indirect CO_2 emission by the grid, it is worth exploring the use of 100 % off-grid renewable solar and wind energy for hydrogen production combined with hydrogen storage. Off-grid solar and wind energy are inherently variable, but DRI plants typically require continuous operation to maximize profitability. As a result, seasonal storage is necessary for hydrogen supply chains relying on 100 % RES. For large-scale seasonal energy storage, hydrogen storage could be more cost-effective than electricity storage, especially for hydrogen consumer like DRI plants [7]. Pimm et al. [7] assessed the energy system requirement of an H2-DRI-EAF plant with solar and wind energy as the power sources in the UK. They found that the required hydrogen storage capacity to buffer the variable renewable energy accounts for ~20 % and ~ 30 % of the total hydrogen energy supplied to the H2-DRI plant for wind and solar sources, respectively. The most common high-density hydrogen storage technologies include compressed gaseous hydrogen (CGH_2) and liquified hydrogen (LH_2). The material-based hydrogen storage technologies, e.g., ammonia (NH_3)-based, methanol (CH_3OH)-based, and liquid organic hydrogen carrier (LOHC)-based, are alternatives with the merits, including easy handling conditions and the possibility of using existing infrastructure. Previous studies [7,14–17] mainly assumed CGH_2 for buffer storage in the hydrogen supply chain from variable solar or wind energy to the DRI plant, but the techno-economic competitiveness of the storage technologies is unclear. When a DRI plant is located far from off-grid solar or wind energy,

hydrogen storage could be implemented at different locations. For example, available caverns for underground CGH_2 storage could be on-site at the DRI plant, at the RES site, or in the middle. However, there is a lack of comparative studies on the techno-economic performance of supply chains with different hydrogen storage locations is lacking, as previous studies [16,17] have considered only a single location.

Besides on-site solar or wind sources at the DRI plant, as assumed in [7,14,15], RES could be located in distant regions. Favorable distant renewable energy locations include offshore wind energy, typically located tens of kilometers from the shore; onshore solar and wind energy in resource-rich regions on the same continent, that is normally hundreds to thousands of kilometers away; and oversea renewables, which may be thousands of kilometers away. When off-grid solar or wind energy is distant from the DRI plant, energy transport becomes necessary. Ortiz Cebolla et al. [17] assessed the techno-economic performance of delivering 1 Mt. of renewable hydrogen per year to a H_2-DRI plant over a distance of 2500 km. Their study compared different hydrogen delivery options, including CGH_2, LH_2, ammonia, methanol, and LOHC, via shipping and pipeline route. The delivery cost included conditioning, reconditioning, and hydrogen transport but excluded the hydrogen production and seasonal storage costs. Devlin and Yang [16] evaluated the techno-economic performance of shipping ammonia and liquid hydrogen as carriers of renewable hydrogen from Australia to Japan. In addition to hydrogen transport, electricity transport via cables is another option for large-scale energy transport [18]. However, insights into the competitiveness of hydrogen transport versus electricity transmission for delivering energy from distant renewable sources to the DRI plants remains limited, as previous studies primarily focused on hydrogen transmission. Furthermore, the costs of off-grid hydrogen delivery under different geographic configurations of RES and DRI plants remain unclear. For example, previous studies [16,17] did not assess the hydrogen supply from dedicated offshore wind farms to steelmaking plants.

The literature overview indicates that the techno-economic competitiveness of potential hydrogen supply chains from distant off-grid solar or wind sources to a DRI plant remains unclear, as previous studies have overlooked several possible configurations. This study seeks to bridge this knowledge gap by addressing the following research question,

What are promising hydrogen supply chains from distant off-grid solar or wind sources to a DRI plant?

To answer this question, this study systematically evaluates and compares the energy efficiency and cost of the hydrogen supply chains incorporating seasonal hydrogen storage. The analyzed supply chains differ in multiple aspects, including renewable energy location (onshore, offshore, or overseas), renewable energy type (solar or wind), hydrogen storage technologies (CGH_2, LH_2, NH_3, CH_3OH, or LOHC), energy transport technologies (pipeline, truck, ship, or cables), and hydrogen storage locations (at the DRI plant or the RES).

2. Methods and data

Section 2.1 outlines the layout of the designed chains, considering the integrations of different steps within the chains. Section 2.2 presents the overall techno-economic methodology. Sections 2.3–2.5 detail the capacity calculation methods of each chain step and provide the relevant techno-economic data. Section 2.6 defines the energy efficiency and loss rates of the supply chains.

2.1. Chains description

This study designs sixty-one hydrogen supply chains from wind or solar sources to a large DRI plant with an annual demand of 1 Mt. of hydrogen, which is sufficient to support a steel production capacity of 15 Mt. per year. The DRI plant is assumed to operate continuously, as this maximizes the profitability [7,11]. Fig. 1 (a) illustrates the general flow charts of these chains. To account for different geographical relationships between supply and demand, this study considers five RES: onshore wind, onshore solar, offshore wind, overseas wind, and overseas solar. The assumed distance for offshore, onshore, and overseas supply chains are 50 km, 2000 km, and 5000 km, respectively, based on real world scenarios and literature. Recent projects in Europe have primarily been developed in waters with depths between 30 m and 50 m, with an increasing number of projects located between 50 km and 120 km offshore [19]. For onshore transmission, 2000 km is approximately the distance from Inner Mongolia (Northwest China) to Shanghai (East China) [20] or from Southern Europe to Northwestern Europe [17]. For oversea transmission, 5000 km is comparable to the distance from Tunisia to Germany [21], from the MENA region to Germany [22], and from Australia to Singapore [23]. The DRI plant is assumed to be located near the shore, facilitating access to offshore wind electricity and overseas hydrogen transported by ships. Electricity generated from solar or wind energy powers electrolyzers for hydrogen production.

This study considers both electricity transmission and hydrogen transport. With electricity transmission, high voltage direct current (HVDC) cables deliver electricity from the RES site to the DRI plant, where electrolyzers generate hydrogen on-site. With hydrogen transport, hydrogen is produced at the RES site and then transported to the DRI plant via pipeline, trucks, or ships. In the hydrogen transport chains, the hydrogen storage facilities can be located either at the RES site or at the DRI plant, whereas in electricity transmission chains, storage is only at the DRI plant. This study considers five large-scale hydrogen storage technologies: CGH_2, LH_2, NH_3, CH_3OH, and LOHC. The DBT pair (dibenzyltoluene)/perhydro-dibenzyltoluene) is chosen among LOHC carriers for its high heat recovery potential [24] and easy handling [24,25]. Hydrogen from electrolyzers undergoes a conditioning process to increase its energy density before storage. This process includes compression for CGH_2, liquefaction for LH_2, ammonia synthesis for NH_3, and hydrogenation for CH_3OH and DBT. All conditioning processes require electricity, while chemical hydrogen storage technologies also generate heat. Additionally, NH_3 and CH_3OH chains require electricity for nitrogen (N_2) production via air separation units (ASU) and CO_2 capture via direct air capture (DAC), respectively. To ensure a fair techno-economic comparison, all chains must achieve climate neutrality. In CH_3OH chains, CO_2 generated during dehydrogenation process is emitted into the atmosphere, whereas other chains do not emit any CO_2. Among various carbon capture options, this study adopts DAC to offset dehydrogenation emissions in CH_3OH chains, ensuring overall climate neutrality despite DAC not being the most efficient and cost-effective option. Chemical chains and LH_2 chains require an additional reconditioning process to release stored hydrogen, including ammonia cracking in NH_3 chains, dehydrogenation in CH_3OH and DBT chains, and regasification in LH_2 chains. The reconditioning process in chemical chains requires both heat and electricity.

This study designs the supply chains with energy and mass integration strategies. In CGH_2, LH_2, and LOHC chains, shared RES supplies the electricity for both the conditioning process and the electrolyzers, as shown in Fig. 1 (b). In NH_3 and CH_3OH chains, shared RES supplies the electricity for the conditioning process, the ASU or DAC unit, and the electrolyzers as shown in Fig. 1 (c). The reconditioning process relies on waste heat from the steelmaking processes, as shown in Fig. 1 (d). When seasonal storage is on-site at the DRI plant in the LH_2 chains, the boil-off hydrogen can be directly utilized by the DRI plant, as shown in Fig. 1 (e).

This study excludes certain storage and transmission pathways due to the lack of demonstrating projects, reliable techno-economic data, or economic feasibility.

a. HVDC cable and pipeline transmission in overseas chains
b. Pipeline transmission of LH_2
c. Ship transport of CGH_2
d. Offshore hydrogen storage

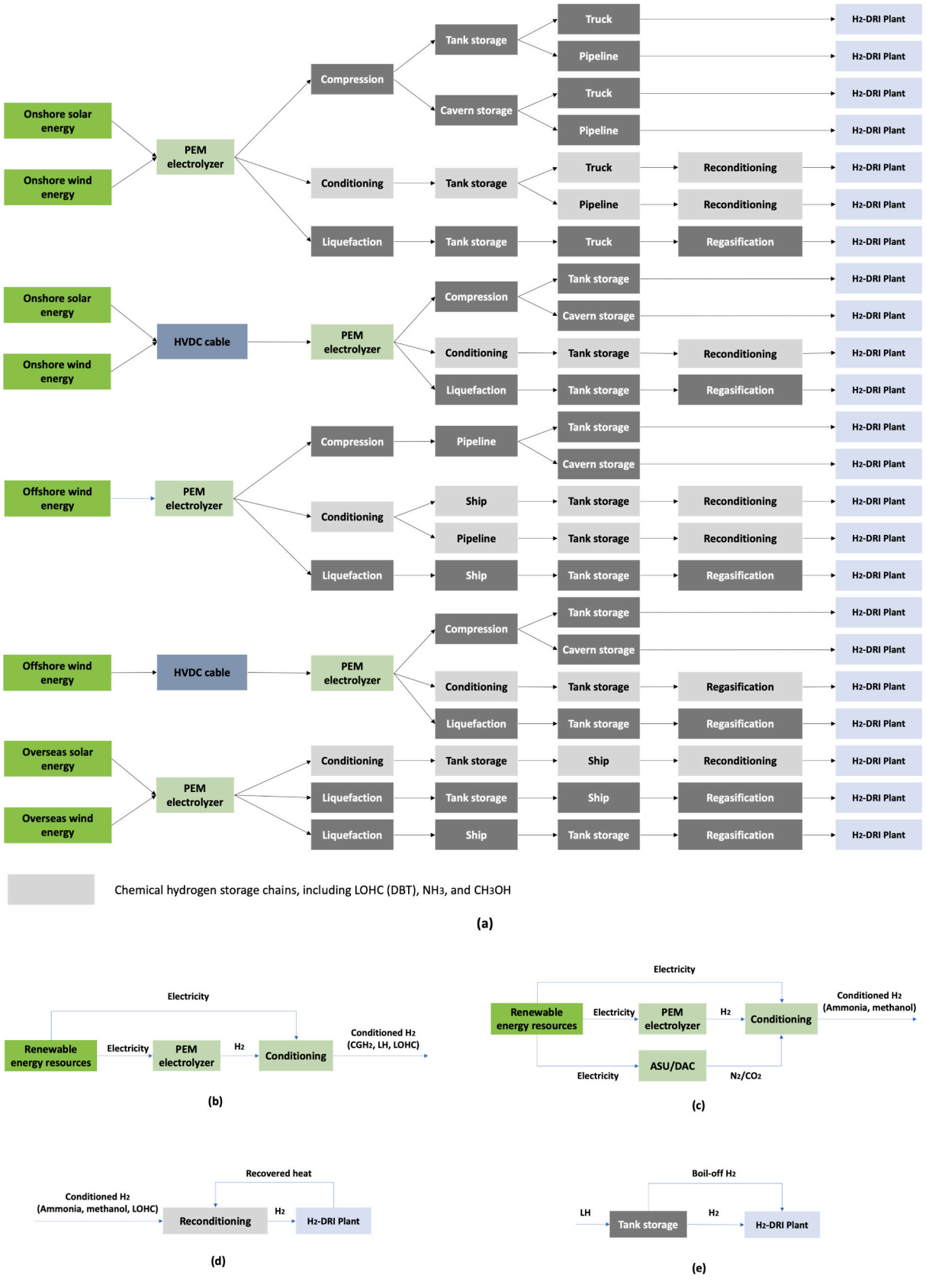

Fig. 1. The flow chart and process integrations of the hydrogen supply chains from RES to an H2-DRI plant. (a) The general flow chart without process integrations. (b) The co-consumption of renewable electricity by the electrolyzers and the conditioning unit in the CGH_2, LH_2, and DBT chains. (c) The co-consumption of renewable electricity by the electrolyzers, the conditioning unit, and the ASU or DAC unit in the NH_3 and CH_3OH chains. (d) The waste heat recovery from the DRI (or other heat sources in the steelmaking plant, e.g., heat from the EAF process) plant for the endothermic reconditioning process in the NH_3, CH_3OH, and DBT chains. (e) Boil-off hydrogen reutilization when the seasonal storage is on-site at the DRI plant in the LH_2 chains.

2.2. Techno-economic analysis methodology

The levelized cost of the hydrogen supply chains, *c_chain*, is the sum of the levelized costs of all the chain steps, including renewable energy generation (*c_RES*), transmission (*c_trans*), electrolyzer (*c_EL*), conditioning (*c_cond*), reconditioning (*c_recond*), carrier production (*c_carrier*), and storage (*c_store*), expressed in $€_{2020}/kg_{H2}$, as shown in Eq. (1).

$$c\_chain = c\_RES + c\_trans + c\_EL + c\_cond + c\_recond + c\_store + c\_carrier \tag{1}$$

Economic input parameters from the literature are first converted to euros (€) using the currency-exchange rate if originally in a different currency. They are then inflation-adjusted to the year 2020 if originally in different year [26,27]. If a publication does not specify the reference year for its data, this study assumes the publication year as the currency reference year.

Eq. (2) calculates the levelized cost of each step.

$$c = \frac{ACAPEX + OPEX}{m\_H_2\_DRI} = \frac{ACAPEX + O\&M + ENEX}{m\_H_2\_DRI \times 8760} \tag{2}$$

where *ACAPEX* is the annuity of the capital expenditures of the chain step, *OPEX* is the annual operational expenditures, which includes the yearly fixed operation and maintenance costs (*O&M*) and the annual energy-related expenses (*ENEX*), and *m_H2_DRI* is the mass rate of hydrogen in kg/h supplied to the DRI plant. Eq. (3) calculates the *ACAPEX* of each technology.

$$ACAPEX = CAPEX\frac{WACC(1+WACC)^n}{(1+WACC)^n - 1} \tag{3}$$

where *CAPEX* is the capital expenditures, *WACC* is the weighted average cost of capital, set at 6 % [28], *n* is the technology-specific lifetime.

For processes without scaling effect, *CAPEX* is calculated as the product of the process capacity and the average unit capital expenditure (*CAPEX_unit*). For processes with scaling effects, Eq. (4) calculates the *CAPEX* of the processes.

$$CAPEX = CAPEX\_base\left(\frac{S}{S\_base}\right)^{\alpha} \tag{4}$$

where *CAPEX_base* is the technology-specific capital expenditure of the base plant size (*S_base*), *S* is the plant size in this study, and α is the scaling factor.

The target year of this study is 2030, meaning that all techno-economic input parameters are projected accordingly.

2.3. Electricity and hydrogen production

The RES-to-electrolyzer capacity ratio affects the overall hydrogen production cost. Increasing this ratio can lead to higher RES curtailment while improving the annual utilization of the installed electrolyzer capacity [29]. To eliminate RES curtailment, this study assumes that the electrolyzer capacity equals the RES capacity. Among the promising electrolyzer technologies, this study selects the proton exchange membrane (PEM) electrolyzer due to its superior adaptability to variable electricity inputs, such as solar or wind power [30].

2.3.1. Capacity calculation

The calculation of electrolyzer and RES capacity incorporates storage and transmission parameters as inputs. In all chains, the conditioning process consistently follows the electrolyzer. The electrolyzer capacity is determined by Eq. (5).

$$P\_EL = \frac{m\_cond \times LHV\_H_2}{\eta\_EL} \tag{5}$$

Where *P_EL* is the electrolyzer input electrical power in kW, *m_cond* is the maximum mass flow rate of hydrogen before entering the conditioning process in kg/h, LHV_H_2 is the lower heat value of hydrogen in kWh/kg, η_EL is the efficiency of the PEM electrolyzer based on LHV_H_2.

In hydrogen transport chains, the renewable energy capacity is the sum of electrolyzer, conditioning, and carrier production electricity inputs, as shown in Eq. (6).

$$P\_RES_{H2trans} = P\_EL_{H2trans} + m\_cond_{H2trans} \times e\_cond_{H2trans} + \frac{m\_cond_{H2trans}}{\rho\_H2} \times e\_carrier_{H2trans} \tag{6}$$

where *P_RES* is the solar or wind power capacity in kW, *e_cond* is the electricity demand by the conditioning process, in kWh/kg_{H2}, *e_carrier* is the electricity demand to capture CO_2 or N_2 from the air in kWh/kg N_2 or kWh/kg CO_2, *e_carrier* = 0 in the CGH_2, LH_2, and DBT chains. ρ_H2 is the mass ratio of H_2 to N_2 (6/28) or CO_2 (6/44) in the conditioning reaction, as shown in Eq. (7) and (8).

$$N_2 + 3H_2 \rightarrow 2NH_3 \tag{7}$$

$$CO_2 + 3H_2 \rightarrow CH_3OH + H_2O \tag{8}$$

In chains with HVDC transmission, RES also compensates for electricity losses in the cables. Eq. (9) calculates the RES capacity for the HVDC chains.

$$P\_RES_{HVDC} = \frac{\left(P\_EL_{HVDC} + m\_cond_{HVDC} \times e\_cond_{HVDC} + \frac{m\_cond_{HVDC}}{\rho\_H2} \times e\_carrier_{HVDC}\right)}{\left(1 - \frac{D}{1000} * l\_HVDC\right)} \tag{9}$$

Where *D* is the transmission distance in km, *l_HVDC* is the electricity loss rate in HVDC cables, in %/1000 km.

2.3.2. Techno-economic data

Table 1 presents the techno-economic parameters for solar and wind electricity generation, as well as electrolyzers. The *CAPEX* data is derived from a projection by Sens et al. based on the experience curve theory. They estimated that, by 2030, the *CAPEX* for PEM electrolyzers, onshore solar, onshore wind, and offshore wind power generation will decrease by approximately 35 %, 30–60 %, 10–30 %, and 10–40 %, respectively, compared to 2020 value [21,31]. The capacity factor (CF) values of RES are representative of countries or regions with favorable solar or wind conditions [19,29]. According to an expert elicitation study on future cost estimation [32], the lifetime of PEM electrolyzers will be 41,000–60,000 h, equivalent to 9–13 years under intermittent operation. This study takes 12 years as the reference value. The electrolyzers' efficiency and operation pressure (50 bar) are also sourced from the expert elicitation study [32]. The cost of seawater desalination

Table 1
Techno-economic parameters for renewable electricity generation from solar or wind and PEM electrolyzers in 2030, the values between the branches show the whole range, and the other is the default value for the calculation.

Parameter	Unit	Onshore PV [19,21,29,31]	Onshore wind [19,21,29,31]	Offshore wind [19,21,29,31]	Electrolyzers [21,30–35]
CAPEX_unit	€$_{2020}$/kW$_{el}$	400 (310–570)	1100 (1010–1240)	1890 (1750–2020)	860 (580–1230)
O&M	%$_{CAPEX}$/year	2.6	2.5	2.8	3.5
n	year	30	30	30	12 (9–13)
CF.	–	0.2	0.4	0.45	
η_EL	%	–	–	–	70 (63–80) [a]
Water cost	€$_{2020}$/kg$_{H2}$	–	–	–	0.02

[a] The efficiency of the electrolyzer is defined as the ratio of LHV of produced hydrogen to the input electrical energy.

plants and water pumped to most areas with water scarcity is estimated to be below 2 €$_{2020}$/m^3 in 2030, contributing less than 0.02 €$_{2020}$/kg$_{H2}$ to the levelized cost of hydrogen [33–35]. This study takes 0.02 €$_{2020}$/kg$_{H2}$ as the cost of water for the electrolyzer.

2.4. Hydrogen conditioning, reconditioning, and storage

Seasonal large-scale hydrogen storage serves as a buffer between intermittent renewable energy sources (RES) and the constant hydrogen demand. The chain steps preceding the hydrogen storage unit operate dynamically, whereas the subsequent steps operate steadily. This study differentiates between the energy capacity and power capacity of hydrogen storage. The energy capacity refers to the maximum annual hydrogen storage in tanks or caverns, while the power capacity represents the peak hydrogen flow rate entering the conditioning or reconditioning process.

2.4.1. Capacity calculation

This study assumes the energy storage capacity as a fixed percentage of the total hydrogen mass entering the seasonal storage annually. This percentage, β in Eq. (10) and Table 2, varies between wind and solar energy sources and is based on a study by Pimm et al. [7]. In all the chains except for the LH_2 chains where the seasonal storage follows the truck or ship, the annual hydrogen mass entering the seasonal storage equals the annual hydrogen mass exiting the conditioning process, and Eq. (10) calculates the energy capacity of the storage.

$$M\_store = m\_cond \times (1 - l\_cond) \times 8760 \times \beta \times CF \quad (10)$$

where *M_store* is the mass of the stored hydrogen annually, *m_cond* is the mass flow rate of the hydrogen entering the conditioning reactor, *l_cond*

Table 2
Techno-economic parameters of the conditioning, carrier production, reconditioning, and storage processes in 2030.

Parameter		Unit	Value				
			CGH_2 [21,36–40]	LH_2 [21,36,39,41]	NH_3 [16,21,41–47]	CH_3OH [21,39,48]	DBT [21,22,24,36]
Conditioning	$CAPEX_{base}$	M€$_{2020}$	0.56 (0.37–1.16)	195 (139–235)	109 (93.4–125)	65.3 (44.2–76.8)	23.4 (19.7–24.1)
	S_{base}	t H_2/d	6	100	100	100	100
	α	–	0.84	0.77	0.85	0.85	0.65
	O&M	%$_{CAPEX}$	5	4	4	4	4
	n	year	20	20	20	20	20
	l_cond	%	0.5 (0–1)	2.2 (1–3.3)	6.5 (0–12.5)	33 (30–35)	0.5 (0–1)
	e_cond	kWh/kg$_{H2}$	0.81	7.4 (6–9.8)	0.7	0.8 (0.7–0.9)	0.2 (0.1–0.3)
	Capex_carrier	€$_{2020}$/kg carrier	–	–	–	–	2.4 (1.7–4.1)
	Carrier lifetime	year	–	–	–	–	15
Carrier production	*CAPEX_unit*	€$_{2020}$/ (t carrier/ year) [b]	–	–	190 (150–230)	400 (390–436)	–
	O&M	%$_{CAPEX}$	–	–	2	4	–
	n	year	–	–	20	25	–
	e_carrier	kWh/kg carrier [b]	–	–	0.11 (0.09–0.13)	1.7 (0.9–2.1)	–
Reconditioning	$CAPEX_{base}$	M€$_{2020}$	–	16.4	63.7 (47.9–105)	21.1 (15.4–44.1)	20.3 (14.8–26.0)
	S_{base}	t H_2/d	–	–	100	100	100
	α	–	–	–	0.85	0.85	0.65
	O&M	%$_{CAPEX}$	–	4	4	4	4
	n	year	–	10	20	20	20
	l_recond	%	–	–	20 (10–30) [a]	−28 (−35 ~ −20)	10 (8–12)
	e_recond	kWh/kg$_{H2}$	–	0.6	3.4 (2.6–4)	4.2 (3.9–4.5)	1.1 (0.7–1.5)
	q_recond	kWh/kg$_{H2}$	–	–	9.7 (8.3–10.1)	3.6 (3.2–4.4)	11.2 (11–12)
Storage	*CAPEX_unit Tank*	€$_{2020}$/kg$_{H2}$	460 (220–600)	41 (18–125)	17 (7–20)	4 (3–6)	8 (6–12)
	Capex_unit UHS	€$_{2020}$/kg$_{H2}$	7 (5–10)	–	–	–	–
	O&M	%$_{CAPEX}$	2	2	2	2	2
	n	year	30	30	30	30	30
	ρ_H2	–	1	1	6/28	6/44	0.062
	l_LH	%/d	–	1.5 (1–2)	–	–	–
	β_{solar} [7]	%	30				
	β_{wind} [7]	%	20				
	t_s [22,36]	days	60				
	m_H$_2$_DRI	kg$_{H2}$/h	31.7				
General information	c_{WasH}	€$_{2020}$/MWh	5 (0–10)				
	c_{ReE}	€$_{2020}$/MWh	55 (40–72)				
	LHV_{H2}	MJ/kg	120				

[a] The loss mainly comes from the hydrogen purification process.
[b] The carrier is CO_2 in the CH_3OH chains or N_2 in the NH_3 chains.

is the hydrogen loss rate in the conditioning process, β is the fixed percentage.

In LH_2 chains, where the seasonal storage follows LH_2 trucks or ships, *m_store* is a fraction of the hydrogen delivered to the seasonal storage by trucks or ships.

$$M\_store = m\_cond \times (1 - l\_cond) \times \left(1 - l\_LH\left(\frac{D}{24v} + \frac{2t\_load}{24}\right)\right) \times 8760 \times \beta \times CF \quad (11)$$

where *v* is the velocity of ships or trucks, in km/h, *t_load* is the loading or unloading duration, in h, *l_LH* is the percentage of liquid hydrogen boil-off losses per day.

In all chains, the conditioning process always precedes seasonal storage and operates dynamically. The conditioning capacity is the maximum hydrogen flow rate entering the conditioning process. Eq. (12) calculates *m_cond* in the CGH_2 chains.

$$m\_cond_{CGH2} = \frac{m\_H_2\_DRI}{(1 - l\_cond)CF} \quad (12)$$

where *CF* is the capacity factor of renewable solar or wind energy.

Eq. (12) also applies in the LH_2 chains with HVDC, as the DRI plant reuses the boil-off hydrogen. In the LH_2 chains with trucks or ships and hydrogen storage on-site at the DRI plant, the trucks or ships also consume part of the hydrogen, and Eq. (13) calculates *m_cond* in these chains.

$$m\_cond_{LH,DRI} = \frac{m\_H_2\_DRI}{CF(1 - l\_cond)\left(1 - l\_LH\left(\frac{D}{24v} + \frac{2t\_load}{24}\right)\right)} \quad (13)$$

In LH_2 chains with trucks or ships and hydrogen storage on-site at the renewable energy site, the boil-off hydrogen is wasted, and Eq. (14) calculates *m_cond* in these chains.

$$m\_cond_{LH,RES} = \frac{m\_H_2\_DRI}{CF\left(1 - \beta \times \left(1 - (1 - l\_LH)^{t_s}\right)(1 - l\_cond)\left(1 - l\_LH\left(\frac{D}{24v} + \frac{2t\_load}{24}\right)\right)\right)} \quad (14)$$

where *t_s* is the hydrogen seasonal storage duration in d.

Eq. (15) calculates *m_cond* in chemical hydrogen storage chains.

$$m\_cond_{chem} = \frac{m\_recond_{chem}}{(1 - l\_cond)CF} \quad (15)$$

where *chem* is the chemical hydrogen storage methods, including NH_3, CH_3OH, and LOHC, *m_recond* is the mass flow rate of the hydrogen embedded in the carriers entering the reconditioning reactor.

The reconditioning process of all chains in this study is located on-site at the DRI plant and operates steadily. Eq. (16) calculates *m_recond*.

$$m\_recond_{chem} = \frac{m\_H_2\_DRI}{1 - l\_recond} \quad (16)$$

Where *l_recond* is the hydrogen loss rate in the reconditioning process.

2.4.2. Techno-economic data

This study considers CGH_2, LH_2, NH_3, CH_3OH, DBT tank storage, and underground hydrogen storage (UHS) for CGH_2. While tank storage exhibits no scaling effect, UHS has a strong one. Reuß et al. [36] applied a scaling factor of 0.28 for UHS in their study. The cost estimation of UHS remains highly uncertainty. Yousefi et al. [37] recently estimated that the *CAPEX* for a 59 kt UHS facility developed in a depleted gas field with a working pressure range of 185–251 bar and a suction pressure of 40 bar is 0.67 (0.58–1.04) $€_{2020}/kg_{H2}$, including compressor and electricity costs. According to the DNV.GL, the LCOH of a 84 kt seasonal hydrogen storage facility is 0.3 $€/kg_{H2}$ [38]. Given that the UHS scale in this study exceeds 84 kt, this study takes the *CAPEX* value from [37] of 7 $€_{2020}/kg_{H2}$ for the reference case.

The chemical hydrogen storage chains require more conversion steps than CGH_2 or LH_2 chains. The DAC facility provides CO_2 for the conditioning process in CH_3OH chains, while the ASU facility provides N_2 in the NH_3 chains. The reconditioning process of the chemical chains requires heat and electricity. The heat demand is met by waste heat recovered from the steelmaking plant, and an external renewable energy plant supplies the electricity for reconditioning. The waste heat is not considered free, as it may hold economic value elsewhere. Due to the lack of readily available data on waste heat costs (c_{WasH} in Table 2), this study assumes a conservative price significantly lower than that of heat from natural gas. Fasihi and Breyer [33] estimated baseload electricity generation costs using variable PV, onshore wind energy, and electricity storage. Under cost-optimized configurations, these costs range from 40 to 72 $€_{2020}$/MWh globally. This study adopts 55 $€_{2020}$/MWh as the reference value for renewable electricity cost (*c_ReE* in Table 2). Eq. (17) calculates the reconditioning *OPEX* in chemical hydrogen storage chains.

$$OPEX\_recond_{chem} = O\&M\_recond_{chem} + m\_recond_{chem} \times e\_recond_{chem} \times c\_ReE^{*}8760 + m\_recond_{chem} \times q\_recond_{chem}{}^{*}c\_WH^{*}8760 \quad (17)$$

where *e_recond* is the electricity demand for the reconditioning process, in kWh/kg_{H2}, *q_recond* is the heat demand for the reconditioning process, in kWh/kg_{H2}, *c_WH* is the cost of waste heat from the steelmaking plant, *c_ReE* is the cost of baseload electricity generated from integrated solar or wind.

Table 2 summarizes the techno-economic input parameters for the conditioning, carrier production, reconditioning, and storage process.

2.5. Transmission

This study considers electricity transmission via HVDC cables and hydrogen transportation via pipelines, tractor-trailer trucks, or ships. For long-distance and large-scale electricity transmission, the mainstream technologies are high voltage alternating current (HVAC) cable and HVDC systems. The HVAC cable suffer from higher dissipative losses and material costs due to the “skin effect” of the alternating current, especially at high voltage and long distances. On average, HVDC transmission losses are approximately 3.5 % per 1000 km, whereas HVAC transmission losses reach 6.7 % under similar conditions [18]. Regarding hydrogen transportation, LH_2 ships and trucks utilize boil-off hydrogen as fuel, the tractor of the CGH_2, NH_3, CH_3OH, and DBT trucks uses renewable hydrogen as fuel. Ammonia ships run on renewable ammonia, while methanol and DBT ships run on renewable methanol. Pipeline transport of CGH_2, NH_3, CH_3OH, and DBT requires compressors to counteract pressure losses. The operating pressure ranges between 6 and 7 MPa in the hydrogen pipeline, 4–8.3 MPa in the NH_3 or CH_3OH

Table 3
Techno-economic parameters of the pipelines in 2030.

Parameter	Unit	Value							
		Onshore [17]				Offshore [c]			
		CGH_2 [21,49]	NH_3	CH_3OH	DBT	CGH_2	NH_3	CH_3OH	DBT
CAPEX_unit [a]	M€$_{2020}$/km	2.5 (2.2–2.8)	0.7 (0.6–0.8)	0.7 (0.6–0.8)	0.32 (0.3–0.35)	5.5 (5.0–6.0)	1.54 (1.4–1.6)	1.54 (1.4–1.6)	0.7 (0.6–0.8)
O&M [b]	%$_{CAPEX}$	5	2.8	2.8	0	8.7	4.9	4.9	0
Lifetime	n	40	40	40	50	40	40	40	50
Diameter	cm	86	45	45	86	86	45	45	86
e_PL [a]	kWh/kg_{H2}/100 km	0.06 (0.032–0.1)	0.02 (0.018–0.022)	0.012 (0.01–0.014)	0.032 (0.028–0.038)	0.06 (0.032–0.1)	0.02 (0.018–0.022)	0.012 (0.01–0.014)	0.032 (0.028–0.038)

[a] The reference value is retrieved from literature, and the range is assumed by the authors.
[b] Except for the *O&M* cost, the pipelines also have an energy cost related to electricity demanded by the compressor stations, and the *ENEX* is calculated as, $ENEX_{PL} = E\_PL \times c\_ReE$.
[c] The offshore pipeline *CAPEX* is 2.2 times the onshore pipeline *CAPEX*, while offshore pipeline *O&M* is 1.75 times the onshore pipeline *O&M* [18].

pipeline, and 1–7 MPa in the DBT pipeline. Integrated solar and wind power systems with electricity storage provide the electricity demand by the compressors.

2.5.1. Capacity calculation

For pipeline transmission, the mass flow rate of hydrogen (in kg_{H2}/h) serves as the capacity indicator. In pipeline chains with hydrogen storage at the renewable energy site, the pipelines operate steadily, and the mass flow rate of hydrogen equals the reconditioning capacity, as shown in Eq. (18).

$$m\_PL_{RES} = m\_recond_{RES} \tag{18}$$

In pipeline chains with hydrogen storage on-site at the DRI plant, the pipelines operate flexibly, and the maximum hydrogen mass flow rate in the pipelines equals the maximum hydrogen mass flow rate exiting the conditioning process, as shown in Eq. (19).

$$m\_PL_{DRI} = m\_cond_{DRI}(1 - l\_cond) \tag{19}$$

Regardless of whether the pipeline operates dynamic or steady, Eq. (20) calculates the recompression electricity demand based on the steady case, since the total annual hydrogen delivery remains unchanged.

$$E\_PL = m\_PL_{RES} \times e\_PL \times \frac{D}{100} \tag{20}$$

where *e_PL* is the electricity demand by the compressors per kg transported hydrogen per 100 km.

For ship or truck transport, the number of trucks or ships is the capacity indicator. The ships or trucks work steadily in all trucks or ship chains with hydrogen storage at the renewable energy site, and Eq. (21) calculates the number of trucks or ships except for that in the LH_2 chains.

$$N_{RES,other} = INT\left(\frac{m\_H_2\_DRI \times \left(\frac{2D}{v} + 2t\_load\right)}{m\_load} \times \frac{8760}{t\_op}\right) + 1 \tag{21}$$

where *m_load* is the payload per truck/ship, *t_op* is the annual operating hours of the truck or ship.

For the chains with LH_2 trucks or ships and hydrogen storage at the renewable energy site, Eq. (22) calculates the trucks or ships' number, considering the boil-off hydrogen in the transmission process.

$$N_{RES,LH} = INT\left(\frac{\frac{m\_H_2\_DRI}{\left(1 - l\_LH\left(\frac{D}{12v} + \frac{t\_load}{12}\right)\right)} \times \left(\frac{2D}{v} + 2t\_load\right)}{m\_load} \times \frac{8760}{t\_op}\right) + 1 \tag{22}$$

When hydrogen storage is on-site at the DRI plant, the maximum number of trucks or ships is N_{RES} divided by the capacity factor, as shown in Eq. (23).

$$N_{DRI} = N_{RES}/CF \tag{23}$$

Additionally, an extra vehicle is needed as buffer storage in the LH_2 chains with ships or trucks.

Table 4
Techno-economic parameters of fuel cell semi-trailer trucks in 2030.

Parameter	Unit	Value [21]					
		Tractor	Trailer				
			LH_2	CGH_2	DBT	CH_3OH	NH_3
CAPEX_unit [a]	k€$_{2020}$/unit	190 (140–270)	910 (740–1530)	680 (520–1060)	110	110	200
O&M	%$_{CAPEX}$	12	2	2	2	2	2
n	year	8	12	12	12	12	12
c_fuel [b]	€$_{2020}$/kWh	0.4	–	–	–	–	–
t_op_{truck}	h	2000	–	–	–	–	–
t_load_{truck}	h	1.5	–	–	–	–	–
v_{truck}	km/h	50	–	–	–	–	–
m_load_{truck}	kg_{H2}/unit	–	4300	1100	1670	2930	2600
e_fuel_{truck}	kWh/km	2.3	–	–	–	–	–

[a] The truck *CAPEX* is the sum of the tractor *CAPEX* and the trailer *CAPEX*, $CAPEX_{truck} = CAPEX\_tractor + CAPEX\_trailer$.
[b] Except for *O&M* cost, the trucks also have an energy cost related to the fuel, and the *ENEX* can be calculate as, $ENEX_{truck} = E\_fuel_{truck} \times c\_fuel$.

Table 5
Techno-economic parameters of HVDC cables in 2030.

Parameter	Unit	Value [18,33,39,50]	
		Onshore	Offshore
$CAPEX_{i,base}$	M€$_{2020}$/km	0.38	2.2
α_i	–	0.6	0.6
$S_{i,base}$	MW	1000	1000
O&M	%$_{CAPEX}$	0.1	0.5
n	year	45	45
$l_{HVDC,1000km}$	%	3.5 (2.5–3.6)	

Eq. (24) calculates the fuel demand in the ship or truck chains except for the LH_2 chains, regardless of whether the vehicles are dynamic or steady.

$$E\_fuel = N_{RES,other} \times t\_op \times v \times e\_fuel \tag{24}$$

where *e_fuel* is the fuel demand by the truck or ship, in kWh/km, which is constant for both loaded or unloaded vehicles.

The HVDC cables always operate flexibly, and the cable capacity (*P_HVDC*) equals *P_RE*, as shown in Eq. (25).

$$P\_HVDC = P\_RE \tag{25}$$

2.5.2. Techno-economic data

Tables 3–6 show the techno-economic parameters for the pipelines, semi-trailer trucks, HVDC cables, and ships.

2.6. Energy efficiency and loss rate

Eq. (26) defines the overall energy efficiency of the chains.

$$\eta = \frac{m\_H_2\_DRI \times LHV\_H_2}{P\_RE \times 8760 \times CF + m\_recond \times (p\_recond + q\_recond) \times 8760 + m\_PL \times p\_PL \times \frac{D}{100} + E\_fuel} \tag{26}$$

where *m_PL* is non-zero only in the pipeline chains, while *E_fuel* is non-zero only in the truck or ship chains.

Energy loss in each chain step is defined as the sum of hydrogen energy loss and energy consumption. Eq. (27) calculates the electrolyzer energy loss.

$$L_{EL} = P\_EL \times (1 - \eta\_EL) \times CF \times 8760 \tag{27}$$

Eq. (28) calculates the energy loss in the conditioning and reconditioning processes.

$$L_{cond\&recond} = 8760(m_{cond} \times p_{cond} \times CF + m_{recond}{}^{*}p_{recond} + m_{recond}{}^{*}q_{recond} + m_{cond} \times l_{cond} \times LHV_{H2} \times CF + m_{recond} \times l_{recond} \times LHV_{H2}) \tag{28}$$

where $m_{recond} = 0$ in the physical chains.

Eq. (29) calculates the energy loss in the carrier production process of the chemical chains.

Table 6
Techno-economic parameters of fuel cell ships in 2030.

Parameter	Unit	Value [21,51]			
		LH_2	DBT	CH_3OH	NH_3
$CAPEX\_unit$	M€$_{2020}$/ship	387 (195–478)	83 (70–96)	83 (70–96)	79 (72–83)
O&M[a]	%$_{CAPEX}$	4	4	4	4
n	year	25	25	25	25
c_fuel	€$_{2020}$/MWh	0	160 (80–240)	160 (80–240)	160 (80–240)
t_op_{ship}	h	8000			
t_load_{ship}	h	54			
v_{ship} *(ship)*	km/h	30			
m_load_{ship}	t H_2/unit	11,000	6600	13,750	9350
e_fuel_{ship}	kWh/km	–	920	920	690

[a] Except for *O&M* cost, the ships also have an energy cost related to the fuel, and the *ENEX* can be calculate as, $ENEX_{ship} = E\_fuel_{ship}{}^{*}c\_fuel$.

$$L_{carrier\ prod} = \frac{m_{cond}}{\rho_{H2}} \times p_{carrier} \times CF \times 8760 \tag{29}$$

Eq. (30) calculates the energy loss in the storage process in the LH_2 chains with seasonal storage on-site at the renewable energy site.

$$L_{store} = \beta \times \left(1 - (1 - l\_LH)^{t_s}\right) \times \frac{m\_H_2\_DRI}{CF(1 - l\_cond)\left(1 - l\_LH\left(\frac{D}{24v} + \frac{t\_load}{12}\right)\right)} LHV\_H_2 \tag{30}$$

Eq. (31) calculates the energy loss in the transmission process.

$$L_{trans} = P\_HVDC \times \frac{D}{1000}{}^{*}(1 - l_{HVDC}) + P\_PL + E\_fuel \tag{31}$$

where *P_HVDC* is non-zero only in the HVDC chains, *P_PL* is non-zero only in the pipeline chains, *E_fuel* is non-zero only in the truck or ship chains.

Eq. (32) calculates the energy loss rate in each chain step.

$$LR_i = \frac{L}{P\_RE \times 8760 \times CF + m\_recond \times (p\_recond + q\_recond) \times 8760 + m\_PL \times p\_PL \times \frac{D}{100} + E\_fuel} \tag{32}$$

3. Results

This section summarizes the key findings from the calculations. Section 3.1 presents energy-related results, while Section 3.2 provides economic analysis. Section 3.3 analyses the impact of input parameters on the LCOH and identifies the input parameters with the most significant impact.

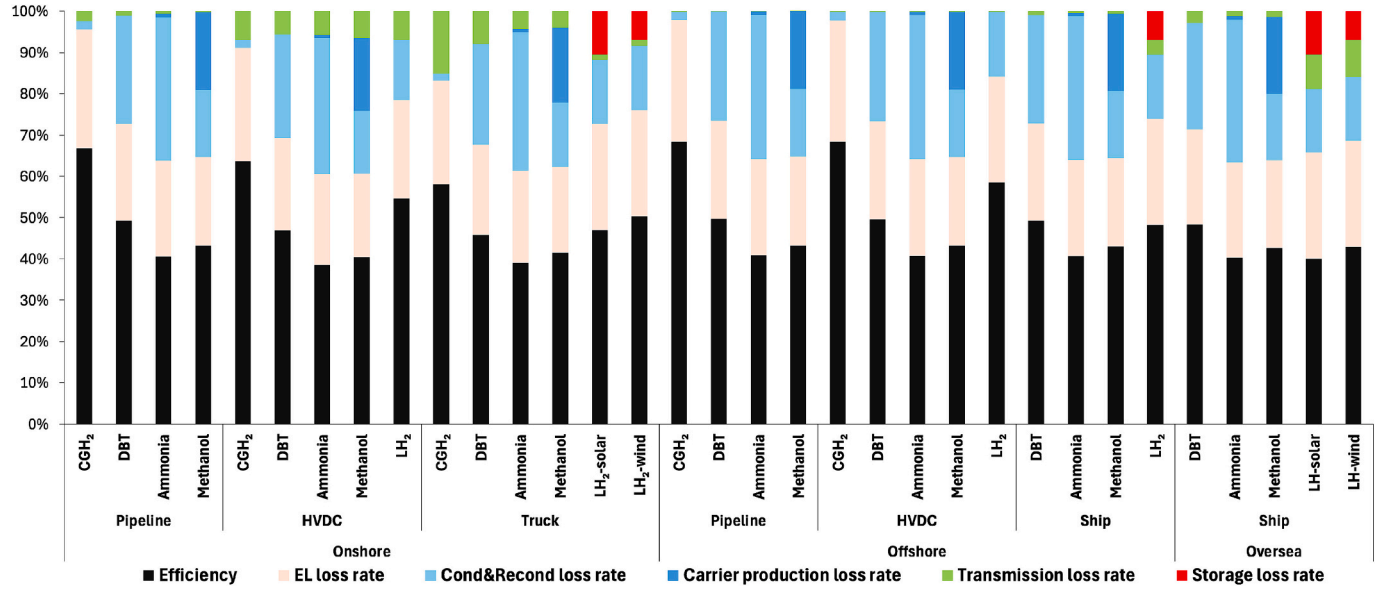

Fig. 2. Overall energy efficiency and loss rate breakdown of the chains.

3.1. Energy results

Fig. 2 illustrates the overall energy efficiency of the chains and the loss rates at each step for thirty-three selected chains, rather than all sixty-one. This selection was made because solar and wind chains exhibit the same efficiency and loss rates when using identical hydrogen storage and transmission methods in both onshore and overseas cases, except for LH_2 chains with ships or trucks. In these LH_2 chains, efficiency differs between solar and wind due to variations in hydrogen storage capacity and boil-off losses. Onshore and overseas chains in Fig. 2 have hydrogen storage at the renewable energy site, whereas offshore chains have storage at the DRI plant. Table 7 presents the capacity and energy demand of each chain step, grouping the chains into eleven categories based on renewable energy source (RES), location, and transmission technology to facilitate comparisons of various hydrogen storage methods. This grouping system will be used throughout the paper for consistency.

The CGH_2 storage chain consistently demonstrates the highest energy efficiency (58.1–68.4 %) among various storage technologies, except in cases involving truck or ship transport. Although the CGH_2 chains exhibit higher transmission losses, they have lower losses in other steps of the supply chain. For instance, in the onshore pipeline configuration, the CGH_2 chain requires 1.2 TWh of energy for transmission, compared to 0.3–0.7 TWh for NH_3, CH_3OH, and DBT pipelines, due to the high operating pressure of the CGH_2 pipeline. Consequently, the CGH_2 pipeline incurs a loss rate of 2.4 %, whereas NH_3, CH_3OH, and DBT pipelines experience losses ranging from 0.4 % to 1.1 %. In the onshore HVDC configuration, the CGH_2 chain exhibits the lowest absolute energy loss in transmission, but its transmission loss rate appears higher because the total energy input of the supply chain is lower than that of alternative chains.

The efficiency ranking among the chemical chains remains consistent in all the groups, following the order: DBT (45.8–49.7 %) > CH_3OH (40.5–43.2 %) > NH_3 (38.5–40.8 %). In the DBT chains, the dominant loss rate is that of the conditioning and reconditioning process (24.3–26.6 %), that is slightly higher than the electrolyzer loss rate (21.8–23.8 %). The NH_3 chain has the lowest efficiency primarily due to its high energy demand and significant hydrogen loss during the conditioning and reconditioning. The lower energy efficiency of the CH_3OH chain is attributed to the substantial energy demand of the carrier production process, i.e., direct air capture of CO_2.

The efficiency of the LH_2 chain is influenced by the transmission method and distance. Under HVDC transmission, LH_2 chain exhibits an efficiency level between that of the CGH_2 and the DBT chains, as the DRI plant can utilize the boil-off hydrogen during storage. In offshore cases involving ship transmission, the LH_2 chain maintains a similar efficiency ranking due to minimal transmission losses resulting from the short transport distance and the presence of hydrogen storage at the DRI plant. However, for the cases involving long-distance transmission of LH_2, e.g., the onshore truck and overseas ship groups, the efficiency declines due to increased hydrogen boil-off during both transmission and storage. In the overseas wind group, it ranks between the CH_3OH and NH_3 chains, while in the overseas solar group, its efficiency is even lower than that of the NH_3 chain.

3.2. Economic results

Fig. 3 illustrates the LCOH and its breakdown across different chain steps under the reference case. The competitiveness of specific chain configurations, including hydrogen storage method, storage location, transmission methods (electricity transmission and hydrogen transport), and RES type (solar and wind), is analyzed in Section 3.2.1–3.2.5. In addition, Section 3.2.5 presents the results under the most conservative and progressive cases.

3.2.1. The competitiveness of hydrogen storage methods

When applicable, the CGH_2-U chain always has the lowest LCOH (3.8–5.6 $€_{2020}/kg_{H2}$) in all the groups except for the onshore truck group. Given that the LCOH of the truck chains is highly sensitive to transmission distance, this study evaluates its impact, as shown in Fig. 4. The CGH_2 chain LCOH decreases more rapidly with the decrease in transmission distance. When the transmission distance is below 500 km in the wind chains (750 km in the solar chains), the CGH_2 chain achieves the lowest LCOH.

The application of UHS depends on whether the specific geophysical conditions are suitable for building a UHS facility, making a secondary option necessary when UHS is unavailable. In the offshore and overseas ship groups where CGH_2 transmission is assumed to be impossible, the DBT chain has the lowest LCOH (5.3–7.5 $€_{2020}/kg_{H2}$). In other groups except for the onshore truck group, the DBT chain has the second lowest LCOH. As illustrated by Fig. 4, when the transmission distance reaches a certain value in the onshore truck group, DBT also has the second lowest LCOH.

In all the groups, the LCOH ranking of the chemical chains aligns

Table 7
Capacity and energy demand of the chain steps.

Chains			Capacity of						Energy demand of				
			RES (GW_{el})	Electrolyzer (GW_{el})	Conditioning (kt H_2/day)	Transmission [a]	Reconditioning (kt/day)	Storage (Mt)	Conditioning electricity (GW_{el})	Carrier electricity (GW_{el})	Reconditioning electricity (GW_{el})	Reconditioning heat (GW_h)	Transmission energy (TWh)
Onshore wind	Pipeline	CGH_2	13.9	13.7	6.9	1.0	–	0.20	0.2	–	–	–	1.2
		NH_3	18.6	18.2	9.2	1.3	3.4	0.25	0.27	0.2	0.5	1.4	0.5
		CH_3OH	20.6	15.8	8.0	1.2	2.1	0.16	0.3	4.5	0.4	0.3	0.3
		DBT	15.2	15.2	7.6	1.1	3.0	0.22	0.06	–	0.1	1.4	0.7
	HVDC	CGH_2	14.9	13.7	6.9	14.9	–	0.20	0.2	–	–	–	–
		LH_2	17.3	13.9	7.0	17.3	2.7	0.2	2.1	–	0.07	–	–
		NH_3	20.0	18.2	9.2	20.5	3.4	0.25	0.27	0.2	0.5	1.4	–
		CH_3OH	22.2	15.8	8.0	22.2	2.1	0.16	0.3	4.5	0.4	0.3	–
		DBT	16.4	15.2	7.6	16.4	3.0	0.22	0.06	–	0.1	1.4	–
	Truck	CGH_2	13.9	13.7	6.9	37,727	–	0.2	0.2	–	–	–	8.7
		LH_2	18.7	16.2	8.2	9918	2.7	0.23	2.5	–	0.06	–	0
		NH_3	18.6	18.2	9.2	19,952	3.4	0.25	0.27	0.2	0.5	1.4	3.5
		CH_3OH	20.6	15.8	8.0	11,066	2.1	0.16	0.3	4.5	0.4	0.3	3.1
		DBT	15.2	15.2	7.6	16,717	3.0	0.22	0.06	–	0.1	1.4	5.5
Onshore solar	Pipeline	CGH_2	27.8	27.3	13.8	1.0	–	0.30	0.5	–	–	–	1.2
		NH_3	37.3	36.3	18.3	1.3	3.4	0.38	0.5	0.5	0.5	1.4	0.5
		CH_3OH	41.2	31.7	16.0	1.2	2.1	0.23	0.5	9.0	0.4	0.3	0.3
		DBT	30.5	30.4	15.3	1.1	3.0	0.33	0.1	–	0.1	1.4	0.7
	HVDC	CGH_2	29.9	27.3	13.8	29.9	–	0.30	0.5	–	–	–	–
		LH_2	34.5	27.8	14.0	34.5	2.7	0.30	4.3	–	0.07	–	–
		NH_3	40.0	36.3	18.3	41.1	3.4	0.38	0.5	0.5	0.5	1.4	–
		CH_3OH	44.4	31.7	16.0	44.4	2.1	0.23	0.5	9.0	0.4	0.3	–
		DBT	32.8	30.4	15.3	32.8	3.0	0.33	0.1	–	0.1	1.4	–
	Truck	CGH_2	27.8	27.3	13.8	37,727	–	0.30	0.5	–	–	–	8.7
		LH_2	40.1	34.8	17.5	9918	2.7	0.38	5.4	–	0.06	–	0
		NH_3	37.3	36.3	18.3	19,952	3.4	0.38	0.5	0.5	0.5	1.4	3.5
		CH_3OH	41.3	31.7	16.0	11,066	2.1	0.23	0.5	9.0	0.4	0.3	3.1
		DBT	30.5	30.4	15.3	16,717	3.0	0.33	0.1	–	0.1	1.4	5.5
Offshore wind	Pipeline	CGH_2	12.3	12.1	6.1	2.2	–	0.20	0.2	–	–	–	0.07
		NH_3	16.6	16.1	8.1	3.0	3.4	0.25	0.2	0.2	0.5	1.4	0.5
		CH_3OH	18.3	14.1	7.1	2.6	2.1	0.16	0.2	4.5	0.4	0.3	0.3
		DBT	13.5	13.5	6.8	2.5	3.0	0.22	0.06	–	0.1	1.4	0.7
	HVDC	CGH_2	12.3	12.1	6.1	12.3	–	0.20	0.2	–	–	–	–
		LH_2	14.3	12.4	6.2	14.3	2.7	0.20	1.9	–	0.07	–	–
		NH_3	16.6	16.1	8.1	17.0	3.4	0.25	0.2	0.2	0.5	1.4	–
		CH_3OH	18.4	14.1	7.1	18.7	2.1	0.16	0.2	4.5	0.4	0.3	–
		DBT	13.6	13.5	6.8	13.6	3.0	0.22	0.06	–	0.1	1.4	–
	Ship	LH_2	17.4	15.0	7.6	3	2.7	0.24	2.4	–	0.06	–	0
		NH_3	16.6	16.1	8.1	3	3.4	0.25	0.2	0.2	0.5	1.4	0.07
		CH_3OH	18.3	14.1	7.1	3	2.1	0.16	0.2	4.5	0.4	0.3	0.07
		DBT	13.5	13.5	6.8	4	3.0	0.22	0.06	–	0.1	1.4	0.14
Overseas wind	Ship	LH_2	22.0	19.0	10.2	7	2.7	0.27	2.9	–	0.06	–	0
		NH_3	18.6	18.2	9.2	7	3.4	0.25	0.2	0.2	0.5	1.4	0.7
		CH_3OH	20.6	15.8	8.0	6	2.1	0.16	0.3	4.5	0.4	0.3	0.7
		DBT	15.2	15.2	7.7	10	3.0	0.22	0.06	–	0.1	1.4	1.4
Overseas solar	Ship	LH_2	47.2	40.9	22.2	10	2.7	0.44	6.3	–	0.06	–	0
		NH_3	37.3	36.3	18.3	8	3.4	0.38	0.5	0.5	0.5	1.4	0.7
		CH_3OH	41.3	31.7	16.0	7	2.1	0.23	0.5	9.0	0.4	0.3	0.7
		DBT	30.5	30.4	15.3	10	3.0	0.33	0.1	–	0.1	1.4	1.4

[a] The unit for the pipeline is Mt./year, truck or ship is the number, and HVDC is GW_{el}.

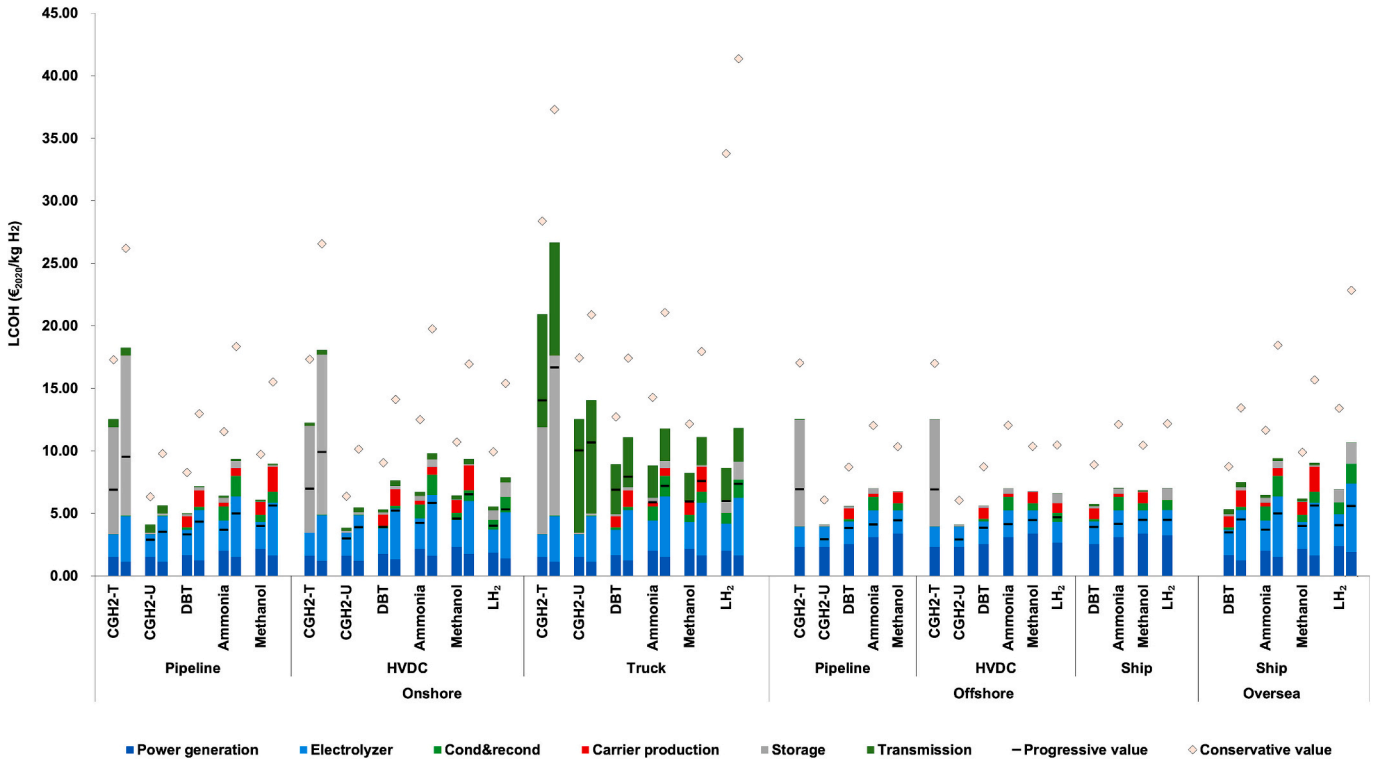

Fig. 3. LCOH and cost breakdown of the chains. The left bar represents the wind chain, while the right bar represents the solar chain in the onshore and overseas groups.

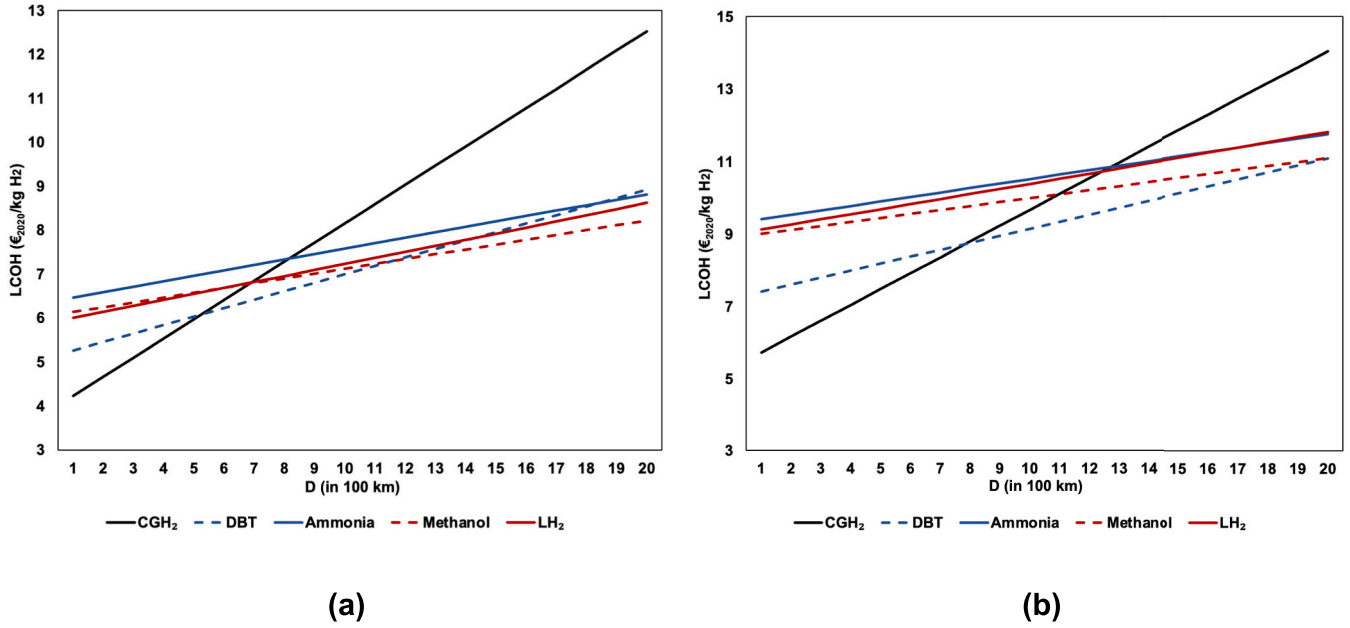

Fig. 4. Effects of transmission distance on the LCOH of the onshore truck wind (a) and solar (b) chains.

with their total loss rate ranking, i.e., DBT < CH_3OH < NH_3. Since the costs of electrolyzer and power generation from RES constitute the primary component of the LCOH, the higher loss rate in the CH_3OH and NH_3 chains result in increased capacity requirement of electrolyzers and RES, thereby leading to a higher LCOH. The LCOH of the CGH2-T chains is exceptionally high at 12.2–26.7 $€_{2020}/kg_{H2}$, primarily due to the high *CAPEX* of the high-pressure tanks.

3.2.2. *The competitiveness of hydrogen storage location*

The onshore and oversea chains with trucks or ships in Fig. 3 incorporate on-site hydrogen storage at the RES site. For CGH_2 and chemical chains, placing hydrogen storage at the renewable site ensures stable operation of the trucks or ships, thereby reducing costs. However, in LH_2 chains, this approach results in boil-off losses, which must be compensated by additional renewable energy production. Fig. 5 (a) compares the LCOH of the overseas chains with hydrogen storage located either at the DRI plant or at the RES site. Storing hydrogen at the

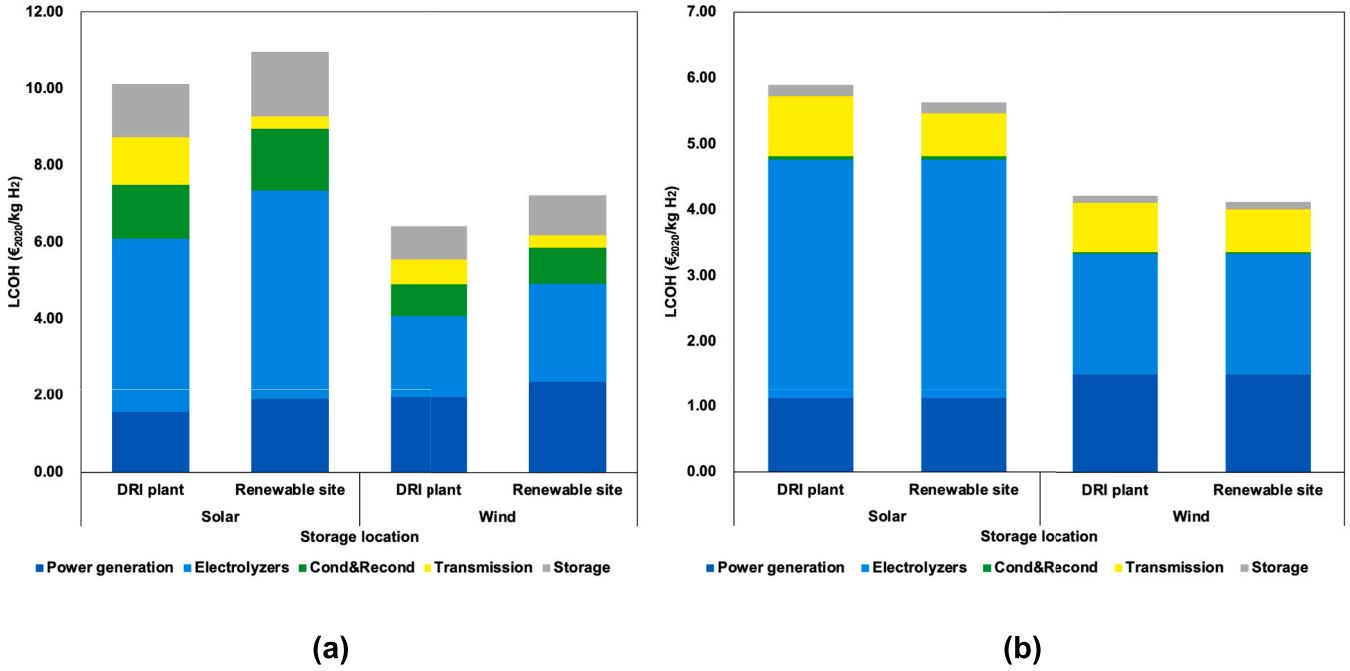

Fig. 5. Effects of storage location on LCOH in the overseas LH_2 chains (a) and the onshore CGH_2 pipeline chains (b).

DRI site leads to a lower LCOH, as the reduction in shipping costs outweighs the additional cost in production and storage costs compared to hydrogen storage at the RES site.

Given the high uncertainty in the real-world location of UHS due to geophysical conditions, this study evaluates the impact of UHS location on the LCOH in the onshore pipeline CGH_2 chain, as shown in Fig. 5 (b). When hydrogen storage is placed at the DRI site, the transmission costs increase by 0.5 $€_{2020}/kg_{H2}$, as the pipelines work flexibly, necessitating a higher installed capacity. Nevertheless, even when storage is located at the DRI site, the LCOH of chains utilizing UHS remains more competitive than other storage methods.

3.2.3. *The competitiveness of electricity transmission and hydrogen transport*

This study presents a case study on the techno-economic competitiveness of electricity transmission versus hydrogen transport, considering the conditions of a hydrogen consumer and a transmission distance of 2000 km, by comparing the onshore HVDC group and the onshore pipeline group. As shown in Fig. 2, electricity transmission via HVDC with hydrogen storage at the DRI site results in a lower LCOH than the CGH_2 pipeline transmission with hydrogen storage at the RES site, despite the HVDC chain having a lower efficiency than the pipeline chain. The primary reason is that the CGH_2 pipeline *CAPEX* is higher than that of the HVDC cable. However, for the chains with chemical hydrogen storage, the pipeline chain achieves a lower LCOH than the HVDC chain, with a difference at 0.3–0.5 $€_{2020}/kg_{H2}$.

3.2.4. *Competitiveness of solar and wind RES*

The LCOH of solar-based hydrogen supply chains is consistently higher than that of wind-based chains with the same RES location, with

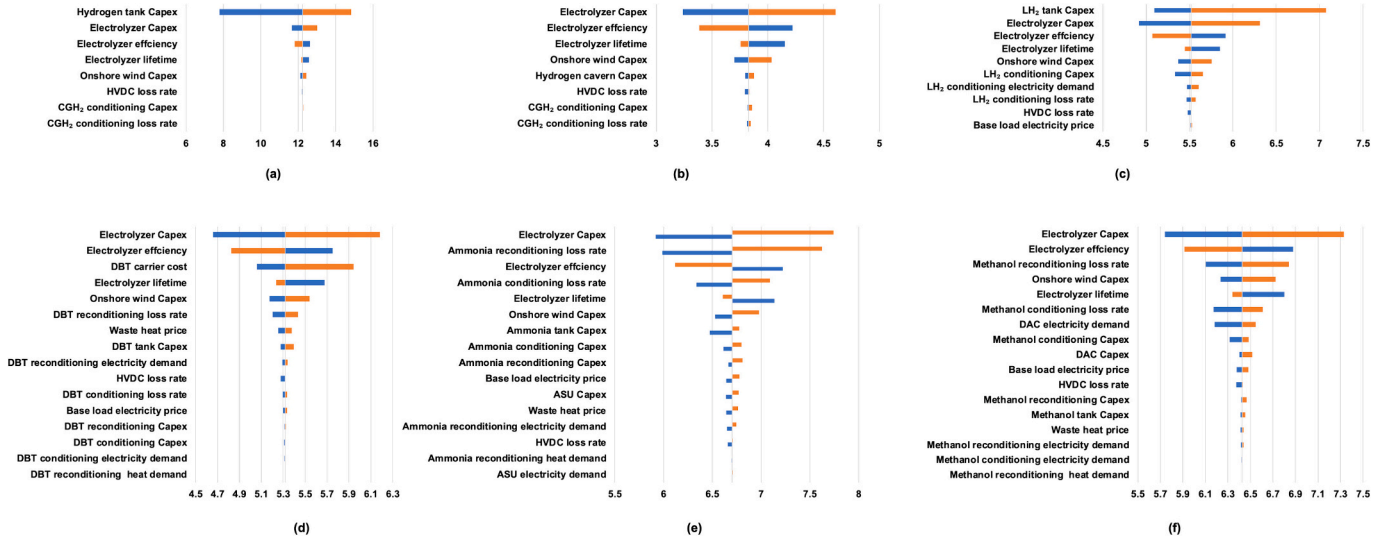

Fig. 6. Sensitivity of the LCOH ($€_{2020}/kg_{H2}$) to the input parameters of the chains belonging to the onshore-wind-HVDC group. (a) the CGH_2-U chain, (b) the CGH_2-T chain, (c) the LH_2 chain, (d) the LOHC chain, (e) the NH_3 chain, (f) the CH_3OH chain.

a LCOH difference ranging from 1.5 to 5.8 €$_{2020}$/kg H_2. Despite the lower cost of solar power generation, the lower solar capacity factor necessitates a higher electrolyzer capacity. Since electrolyzer costs constitute a significant portion of the total expenditure, this results in a higher LCOH for solar-based chains. Additionally, solar-based supply chains require larger hydrogen storage capacities compared to their wind-based counterparts.

The cost advantage of wind-based supply chains persists even when comparing different RES locations. For instance, oversea wind-based supply chains using NH_3, CH_3OH, and DBT achieve lower LCOH than corresponding onshore solar supply chains with pipeline transmission, despite the longer transport distances and higher transmission costs. This underscores the critical role of renewable resource availability in shaping cost-effective hydrogen supply chains. For a region with limited wind resources and no underground hydrogen storage facilities, importing hydrogen from other regions with abundant wind resources could achieve a lower cost of hydrogen supply.

3.2.5. *The most conservative and most progressive results*

Fig. 3 also presents the LCOH under the most conservative and progressive case. This study accounts for the uncertainties in the input parameters, including the *CAPEX*, efficiency, loss rate, lifetime, and energy demand, of several processes. Each parameter has a reference value and a corresponding range, as detailed in Tables 1–6. The most progressive case assumes the highest efficiency and longest lifetime while adopts the lowest *CAPEX*, loss rates, and energy demand. Conversely, the most conservative case follows the opposite assumptions. As shown in Fig. 3, the difference between the maximum and minimum LCOH under these two cases is substantial (from 2.6 to 35 €$_{2020}$/kg$_{H2}$). The variation is primarily driven by the electrolyzer parameters, as discussed in Section 3.3. The competitiveness of different hydrogen storage methods can shift when input values are adjusted within their respective ranges

3.3. *Sensitivity analysis*

In this sensitivity analysis, the variation of LCOH of the chains is examined within the parameter ranges specified in brackets in Tables 1–6, aiming to identify the factors with the most significant effects. Fig. 6 presents the sensitivity analysis results of the onshore-wind-HVDC chains, while results for the remaining chains are provided in the Appendix. The red bars represent the LCOH corresponding to the lower bound of each parameter, whereas the blue bars indicate the LCOH at the upper bound.

As shown in Fig. 3, electrolyzer costs constitute a major component of the LCOH. Sensitivity analysis results show that the electrolyzer parameters have a significant impact LCOH. When EL *CAPEX* increases from 580 to 1230 €$_{2020}$/kW$_{el}$, LCOH of the chains increases by 1.2–4.5 €$_{2020}$/kg$_{H2}$. An increase in EL efficiency from 63 % to 80 % reduces the LCOH of the chains by 0.8–1.8 €$_{2020}$/kg$_{H2}$. Except for a few chains of the onshore truck group, EL *CAPEX* and efficiency rank consistently among the top three factors influencing LCOH. The renewable electricity generation costs also contribute significantly to LCOH, the sensitivity results show that the impact of RE *CAPEX* is lower than EL parameters, primarily due to the narrower range of the RE *CAPEX*.

Parameters related to storage, conditioning, reconditioning, and transmission processes significantly impact specific chains:

- Increasing the C*APEX* of the CGH_2 tanks from 286 to 780 €$_{2020}$/kg$_{H2}$ increases the LCOH by 9.2–13.7 €$_{2020}$/kg$_{H2}$ in the CGH_2 chains, while increasing the LH_2 tanks *CAPEX* from 18 to 125 €$_{2020}$/kg$_{H2}$ increases the LCOH by 2.2–5.1 €$_{2020}$/kg$_{H2}$ in the LH_2 chains.
- In the LOHC chains, the LOHC carrier cost is a critical factor. Increasing the carrier cost from 1.7 to 4.1 €$_{2020}$/kg carrier increases the LCOH by 1.0–1.5 €$_{2020}$/kg$_{H2}$.
- Loss rates during the conditioning and reconditioning process significantly impact NH_3 and CH_3OH chains. In NH_3 chains, the LOHC variation is 0.7–1.2 and 1.7–3.1 €$_{2020}$/kg$_{H2}$ with the change of conditioning loss rate and reconditioning loss rate, respectively. In CH_3OH chains, the variation is 0.4–0.7 and 0.7–1.2 €$_{2020}$/kg$_{H2}$, respectively.
- Increasing the DAC electricity demand from 0.9 to 2.1 kWh/kg carrier increases the LCOH by 0.3–0.5 €$_{2020}$/kg$_{H2}$.

4. Discussion

Section 4.1 compares the results from this study with findings from the literature to validate the quantified outcomes. Given the different chain configurations in previous studies, this comparison also examines the underlying reasons for discrepancies between the results. Section 4.2 presents the final considerations of this study.

4.1. *Comparison with literature*

Sens et al. assessed the hydrogen supply costs from hybrid wind and solar energy to a hydrogen refueling station in Germany under various renewable energy locations (onshore and overseas) and different hydrogen storage methods, including CGH_2, LH_2, DBT, CH_3OH, and NH_3 [21]. Their foundlings indicate that, in 2030, CGH_2 storage and transmission has the lowest LCOH of 5 €$_{2020}$/kg$_{H2}$ for CGH_2 refueling, while LH_2 storage and transmission has the lowest LCOH of 7 €$_{2020}$/kg$_{H2}$ for LH_2 refueling. In comparison, this study finds that the lowest LCOH of the CGH_2 supply chain to the DRI plant is 3.8 €$_{2020}$/kg$_{H2}$, which is relatively lower than the hydrogen refueling station case. Two main factors contribute to this difference. First, UHS has a strong scaling effect with a scaling effect of approximately 0.28 [36], and the *CAPEX* of UHS (7 €$_{2020}$/kg$_{H2}$) in the DRI chain in this study is lower than that (12–128 €$_{2020}$/kg$_{H2}$) in the hydrogen refueling chain in the study by Sens et al. Second, the DRI plant operates at a relatively lower pressure, typically below the pressure in the CGH_2 storage and transmission (100 bar). Consequently, recompression of the hydrogen after the storage and transmission process is not necessary, unlike in the hydrogen refueling station chains, where a pressure level of >700 bar is required for the vehicle refueling [20,21,52].

Steelmaking plants typically generate substantial waste heat [5,53–57], which can be recovered and used in the endothermic hydrogen release process of the chemical hydrogen storage technologies. This reduces costs compared with the hydrogen refueling chains, where waste heat is generally unavailable [58–61]. Sens et al. found that the CH_3OH chain exhibits the lowest LCOH among the chemical chains. However, this study indicates that the DBT chain has the lowest LCOH among the studied chemical chains. The primary reason is the stronger scaling effect for the DBT conditioning and reconditioning processes, with a scaling factor of 0.65. Ortiz Cebolla et al. analyzed various hydrogen storage and transport methods from a stable hydrogen source to a steelmaking plant, considering a hydrogen transport distance of 2500 km via pipeline or ship. Their findings indicate that when waste heat from the steelmaking plant is utilized for LOHC dehydrogenation, the LOHC chain has the lowest delivery cost compared with NH_3 and CH_3OH chains. This conclusion aligns with the findings of this study regarding the competitiveness of chemical hydrogen storage chains.

4.2. Final considerations

The findings of this study are influenced by the sensitivity of the input parameters and assumptions regarding chain configurations. The sensitivity analysis of the input parameters is extensively discussed in Section 3.3. This section, instead of providing a quantitative assessment, introduces possible variations in chain configurations that were not included in Fig. 1 and quantitatively discusses their possible effects.

Further process integration strategies, including heat and mass integration, could enhance the efficiency of hydrogen supply chains. 1) The heat generated during the hydrogenation process in chemical hydrogen carriers could be recovered and reutilized. Given the potential lack of local heat demand near the hydrogenation process, repurposing this heat for electricity generation or hydrogen production represents a promising avenue for further investigation. 2) The oxygen byproduct from electrolysis could be monetized to improve the economic viability of the supply chains. 3) This study assumed that heat demand in the DAC process is electrified, However, in CH_3OH-based chains with HVDC transmission, where the DAC process is located at the steelmaking site, utilizing waste heat from the steelmaking plant could be a viable alternative.

Integrating solar and wind energy while optimizing the RES-to-electrolyzer capacity ratio can reduce hydrogen production costs. In certain regions, such integration can lower renewable power generation costs, electrolyzer capital expenditures, and the required hydrogen storage capacity [7]. Brändle et al. [29] conducted a global assessment of hydrogen production costs from electrolyzers powered by RES and found that the hybrid systems offer only marginal cost advantages in specific geographic locations with certain conditions. Additionally, their study indicates that the LCOH could decrease by 5–20 % with an optimized RES-to-electrolyzer capacity ratio of 1.5–2. This optimization enhances electrolyzer utilization, thereby decreasing its costs contribution to the total LCOH, albeit at the expense of increased RES curtailment.

Several assumptions in this study may lead to an underestimation of the losses and LCOH. 1) This study assumed that the DRI plant is located near the shore, thereby excluding onshore delivery costs in offshore and overseas chains. However, the plant may be situated further inland, increasing transportation costs. 2) In the overseas chains, it is assumed that the RES in the exporting country is located near the harbor, neglecting inland energy transmission costs. In practice, the RES may be situated inland, requiring additional transmission infrastructure, which would decrease the efficiency and increase LCOH. 3) Additional harbor costs may arise in the chains involving maritime transport. In particular, LH_2 chains could incur higher costs due to the need for dedicated infrastructure, unlike the chemical carriers that can leverage existing facilities. 4) This study assumed that the offshore electrolyzer *CAPEX* and Opex, as well as the DAC and ASU *CAPEX* and Opex, are identical to their onshore counterparts. However, offshore chains may require additional costs due to the marine environment conditions. 5) Deliver the heat from the steelmaking plant to the reconditioning process may necessitate additional facilities, such as heat exchangers, pipelines, and pumps. The associated energy demand and cost have not been accounted for in this study. 6) This study assumed significant cost reduction for various technologies by 2030. For instance, the electrolyzer *CAPEX* is projected to be 850 (580–1230) €$_{2020}$/kW$_{el}$, whereas current real-world projects report values exceeding 2000 €$_{2020}$/kW$_{el}$ [62,63]. Similarly, the current *CAPEX* of solar, onshore wind, and offshore wind is 628, 1325, 2840 €$_{2020}$/kW$_{el}$, respectively, according to [31]. Therefore, the findings of this study are contingent on future technological advancements and cost reductions. 7) The operation pressure of the UHS is higher than that of pipelines and electrolyzer, necessitating additional compression work. This study does not account for this compression work in efficiency calculation. 8) Transmission routes may require detours due to geographical and infrastructural constraints, leading to higher transmission cost and lower supply chain efficiency.

5. Conclusion

This study quantifies the techno-economic competitiveness of hydrogen supply chains from off-site wind or solar energy to a hydrogen-based direct reduced iron (H_2-DRI) plant. The analysis is based on the levelized cost of hydrogen for sixty-one chains, which vary by renewable energy type and location, energy storage methods, energy transmission methods, and hydrogen storage location. A mathematical model is developed to evaluate the losses, capacity, and costs of each chain step. The key findings under the reference input parameters are as follows,

1. Compressed gaseous hydrogen (CGH_2) chain with underground hydrogen storage (UHS) has the lowest levelized cost of hydrogen (LCOH) when available, with an LCOH at 3.8–5.5 €2020/kg$_{H2}$, outperforming alternative storage methods, including liquid hydrogen (LH_2), ammonia (NH_3), methanol (CH_3OH), and liquid organic hydrogen carrier (DBT). This cost advantage is primarily due to the strong scaling effect and, therefore, the low cost of UHS.
2. When the CGH_2 chain with UHS is unavailable, DBT chains are the next-best options.
3. CGH_2 chains with tank storage, methanol chains, and ammonia chains are economically less competitive. The reason for the high LCOH for the CGH_2 chains with tank storage is the high *CAPEX* of the high-pressure tanks, for CH_3OH chains is the high energy demand in the direct air capture, and for NH_3 chains is the high hydrogen loss during reconditioning.
4. When using LH_2 for hydrogen storage and transmission, the hydrogen storage location should be placed near the DRI plant. However, in the CGH_2, NH_3, CH_3OH, and LOHC chains, the storage location should be near the renewable energy site.
5. In CGH_2 chains, high voltage direct current (HVDC) cable transmission is preferred above pipeline transport when considering LCOH, whereas in chemical chains, pipeline transport is more cost-effective option.

An extensive sensitivity analysis identifies the parameters with the most significant impact on LOHC across different chains. Hydrogen production parameters play a dominant role in all the chains, with EL *CAPEX* and EL efficiency consistently ranking among the top three factors affecting LCOH. Other key parameters include the tank *CAPEX* in the CGH_2 chains with tank storage and LH_2 chains, LOHC carrier cost in the LOHC chains, loss rates during the conditioning and reconditioning process in NH_3 and CH_3OH chains, and direct air capture (DAC) energy demand in the CH_3OH chains.

This study introduces a general framework for assessing hydrogen supply chains from renewable solar or wind sources to steelmaking, allowing for a comparative assessment of different chain configurations and identification of the most promising options. To ensure a fair comparison, several simplifying assumptions were made, which may differ from real-world scenarios. To address these limitations, future research is recommended in two key areas. First, a more comprehensive assessment of integrated energy systems involving multiple industrial and energy sectors is needed. Although this study incorporates various heat and mass integration strategies, some integration potentials, e.g., the recovery of hydrogenation heat, can only be fully explored within a broader multi-sector energy modeling framework. Second, spatially explicit assessments of hydrogen supply chains should be conducted. Many key input parameters in this study, including solar and wind resource availability, transportation distances, and infrastructure

constraints, are highly dependent on location.

CRediT authorship contribution statement

Longquan Li: Writing – original draft, Software, Methodology, Investigation, Conceptualization. **Purushothaman Vellayani Aravind:** Supervision, Conceptualization. **Annika Boldrini:** Writing – original draft, Resources, Investigation. **Machteld van den Broek:** Writing – original draft, Supervision, Methodology, Investigation, Conceptualization.

Declaration of competing interest

The authors declare that they have no known competing financial interests or personal relationships that could have appeared to influence the work reported in this paper.

Acknowledgments

The authors would like to thank the useful comments from Dr. Johannes Miocic and Ms. Rebeka Beres. The author, Longquan Li, receives the financial support from the scholarship granted by China Scholarship Council (CSC, No. 202106370021).

Appendix A. Appendix

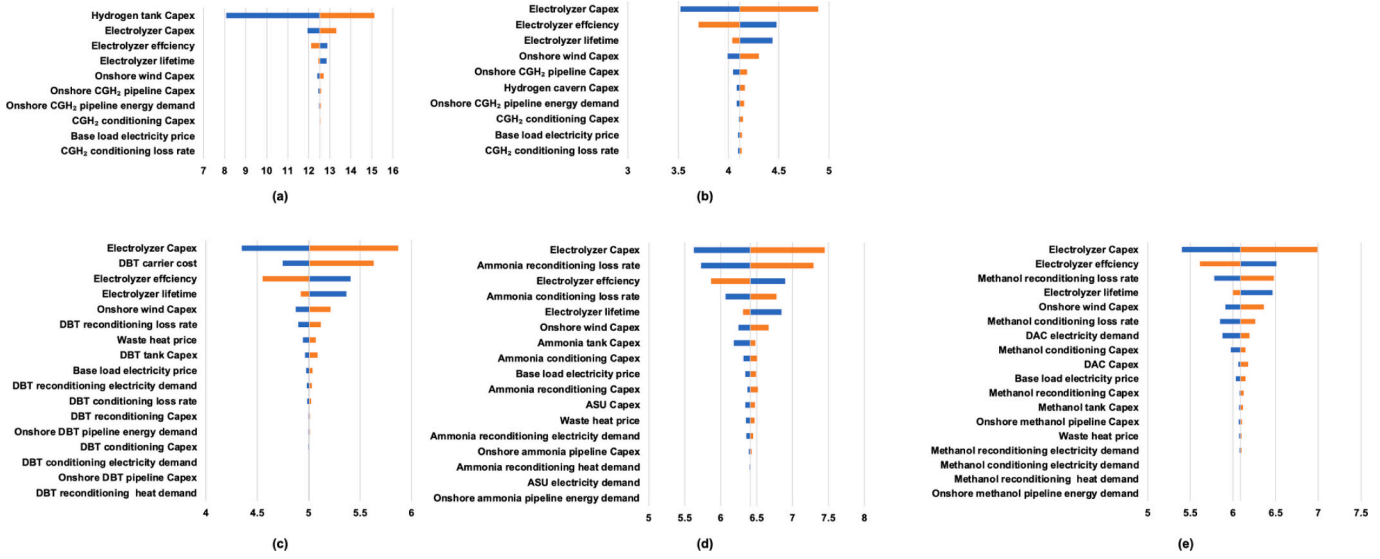

Fig. A1. Sensitivity of the LCOH ($€_{2020}/kg_{H2}$) to the input parameters of the chains belonging to the onshore-wind-pipeline group. (a) the CGH_2-U chain, (b) the CGH_2-T chain, (c) the LOHC chain, (d) the NH_3 chain, (e) the CH_3OH chain.

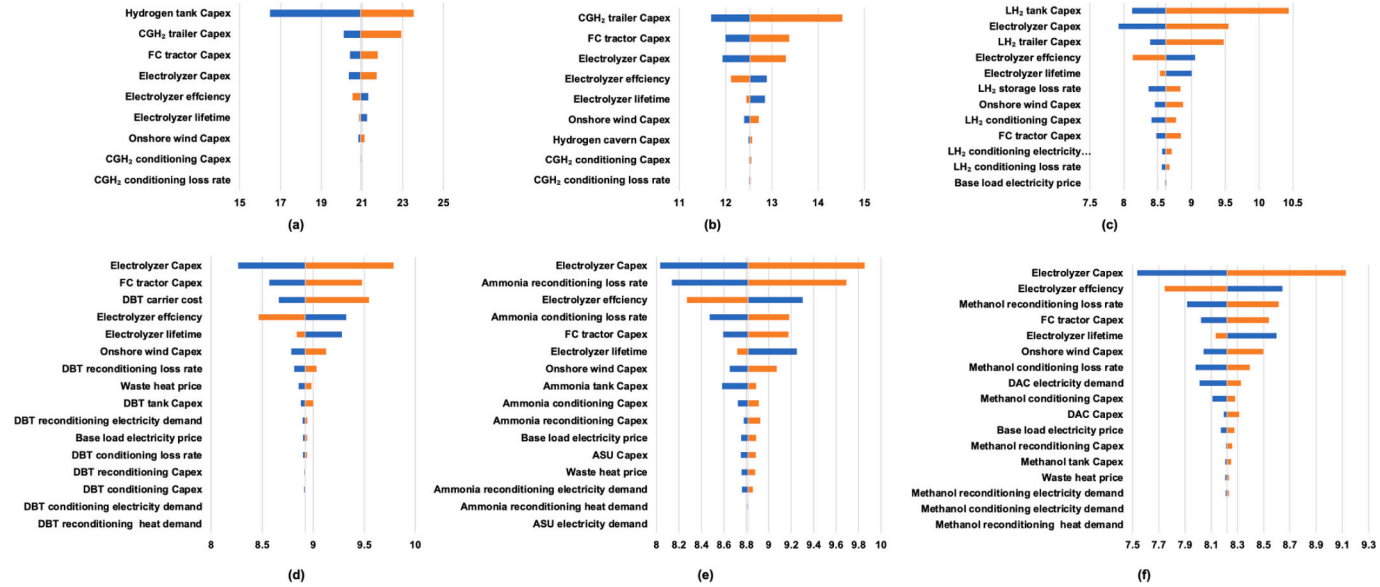

Fig. A2. Sensitivity of the LCOH ($€_{2020}/kg_{H2}$) to the input parameters of the chains belonging to the onshore-wind-truck group. (a) the CGH_2-U chain, (b) the CGH_2-T chain, (c) the LH_2 chain, (d) the LOHC chain, (e) the NH_3 chain, (f) the CH_3OH chain.

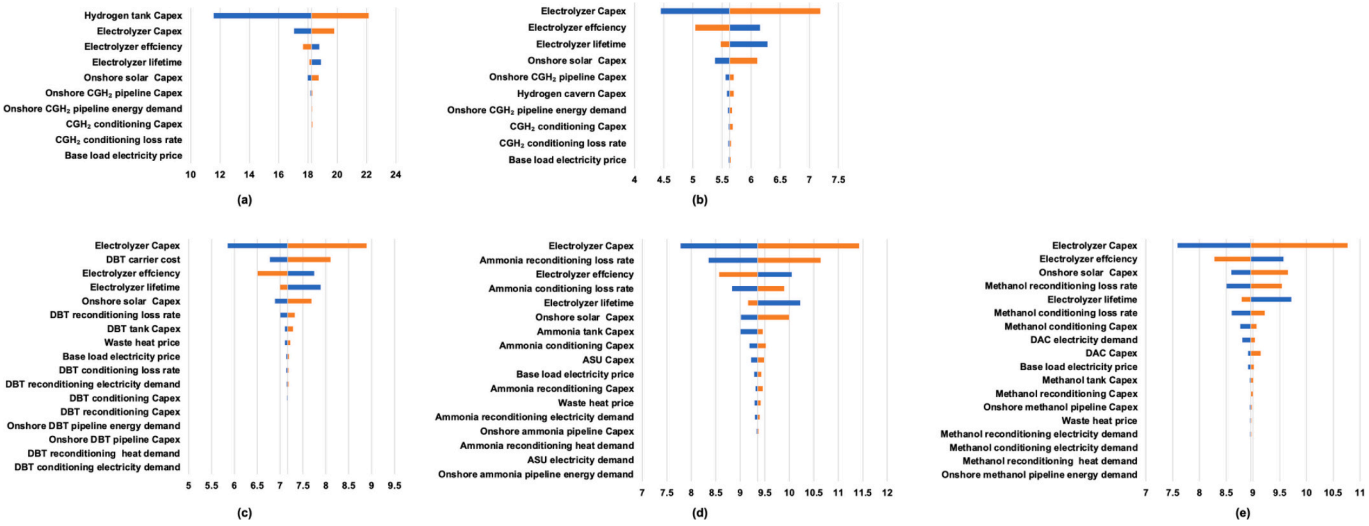

Fig. A3. Sensitivity of the LCOH ($€_{2020}/kg_{H2}$) to the input parameters of the chains belonging to the onshore-solar-pipeline group. (a) the CGH_2-U chain, (b) the CGH_2-T chain, (c) the LOHC chain, (d) the NH_3 chain, (e) the CH_3OH chain.

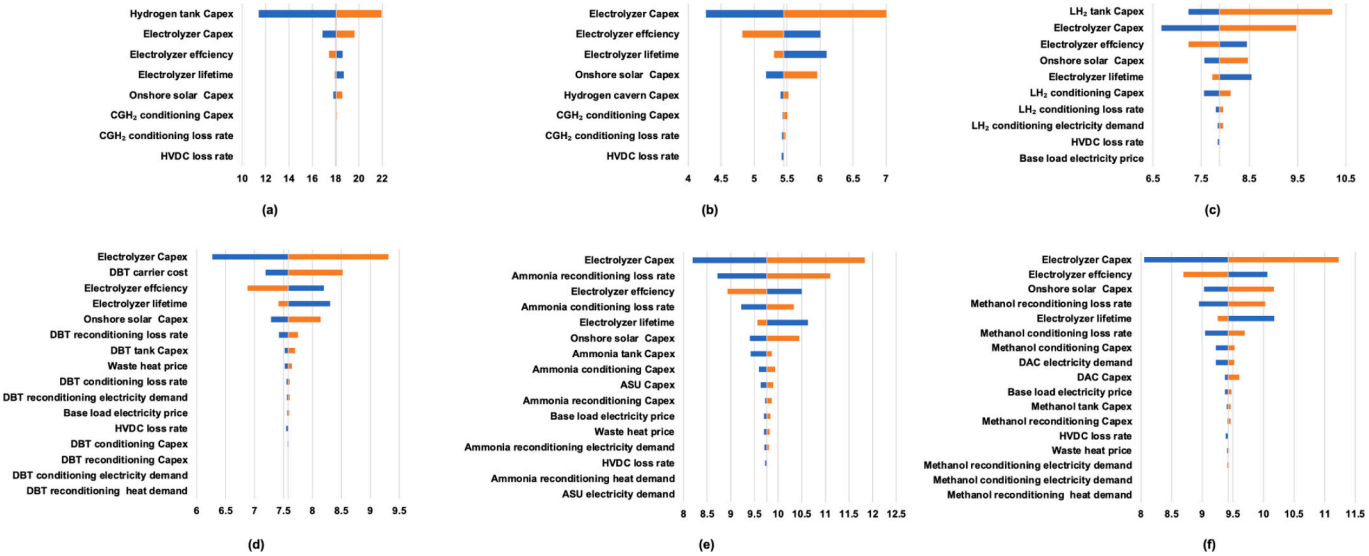

Fig. A4. Sensitivity of the LCOH ($€_{2020}/kg_{H2}$) to the input parameters of the chains belonging to the onshore-solar-HVDC group. (a) the CGH_2-U chain, (b) the CGH_2-T chain, (c) the LH_2 chain, (d) the LOHC chain, (e) the NH_3 chain, (f) the CH_3OH chain.

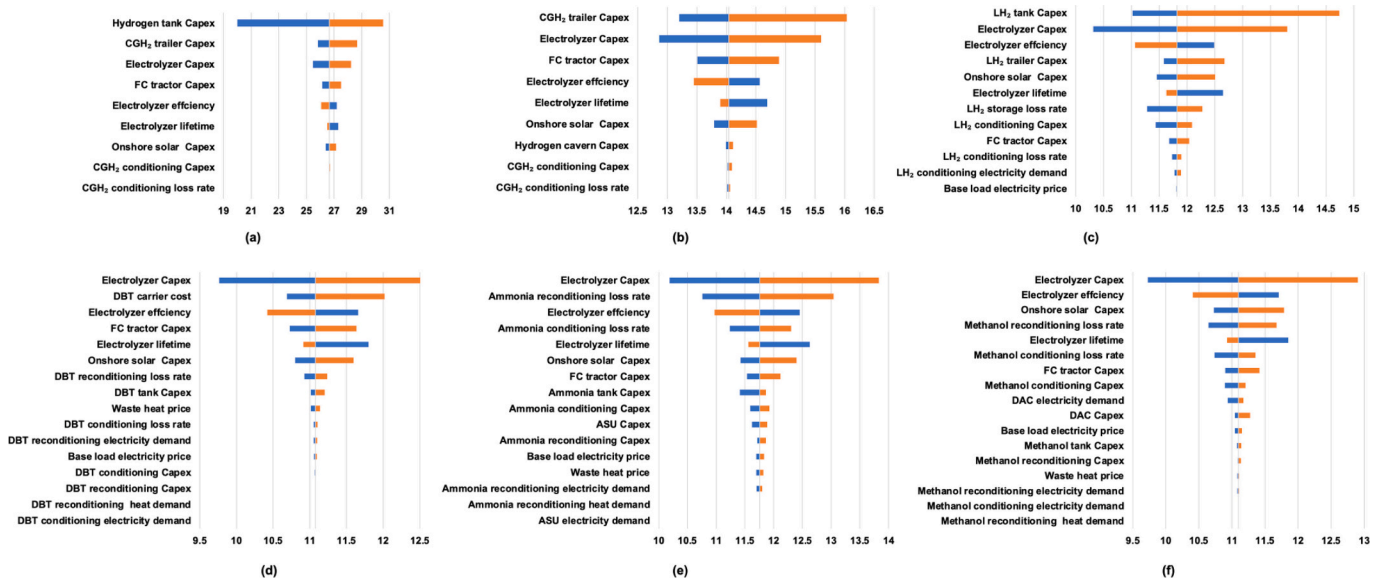

Fig. A5. Sensitivity of the LCOH ($€_{2020}/kg_{H2}$) to the input parameters of the chains belonging to the onshore-solar-truck group. (a) the CGH_2-U chain, (b) the CGH_2-T chain, (c) the LH_2 chain, (d) the LOHC chain, (e) the NH_3 chain, (f) the CH_3OH chain.

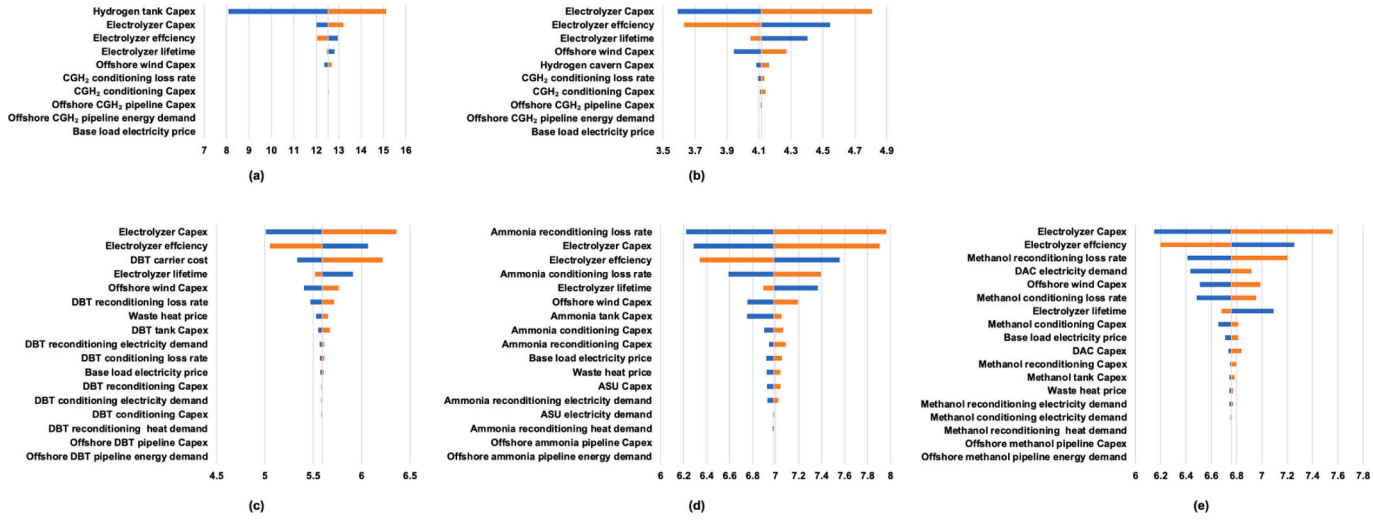

Fig. A6. Sensitivity of the LCOH ($€_{2020}/kg_{H2}$) to the input parameters of the chains belonging to the offshore-pipeline group. (a) the CGH_2-U chain, (b) the CGH_2-T chain, (c) the LOHC chain, (d) the NH_3 chain, (e) the CH_3OH chain.

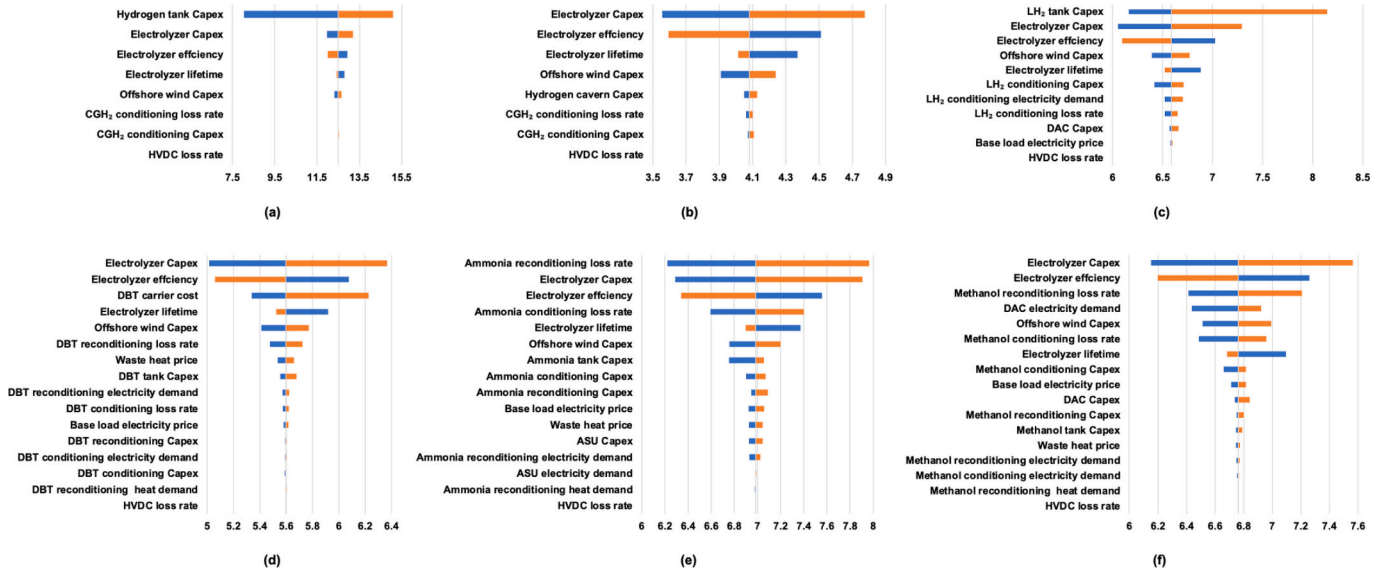

Fig. A7. Sensitivity of the LCOH ($€_{2020}/kg_{H2}$) to the input parameters of the chains belonging to the offshore-HVDC group. (a) the CGH_2-U chain, (b) the CGH_2-T chain, (c) the LH_2 chain, (d) the LOHC chain, (e) the NH_3 chain, (f) the CH_3OH chain.

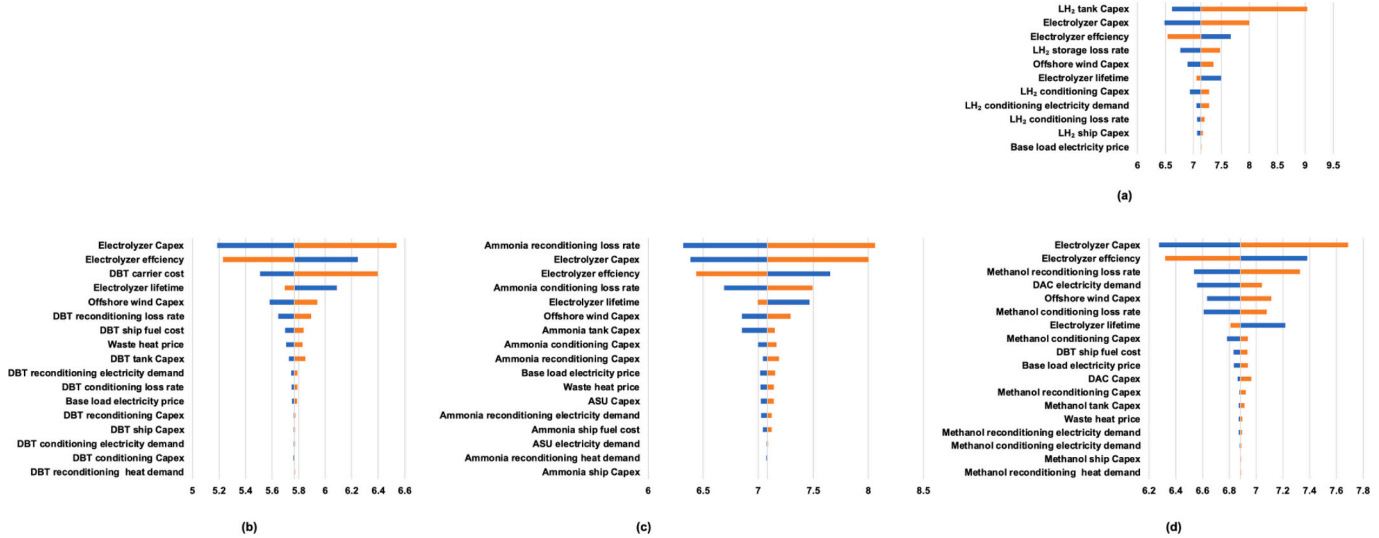

Fig. A8. Sensitivity of the LCOH ($€_{2020}/kg_{H2}$) to the input parameters of the chains belonging to the offshore-ship group. (a) the LH_2 chain, (b) the LOHC chain, (c) the NH_3 chain, (d) the CH_3OH chain.

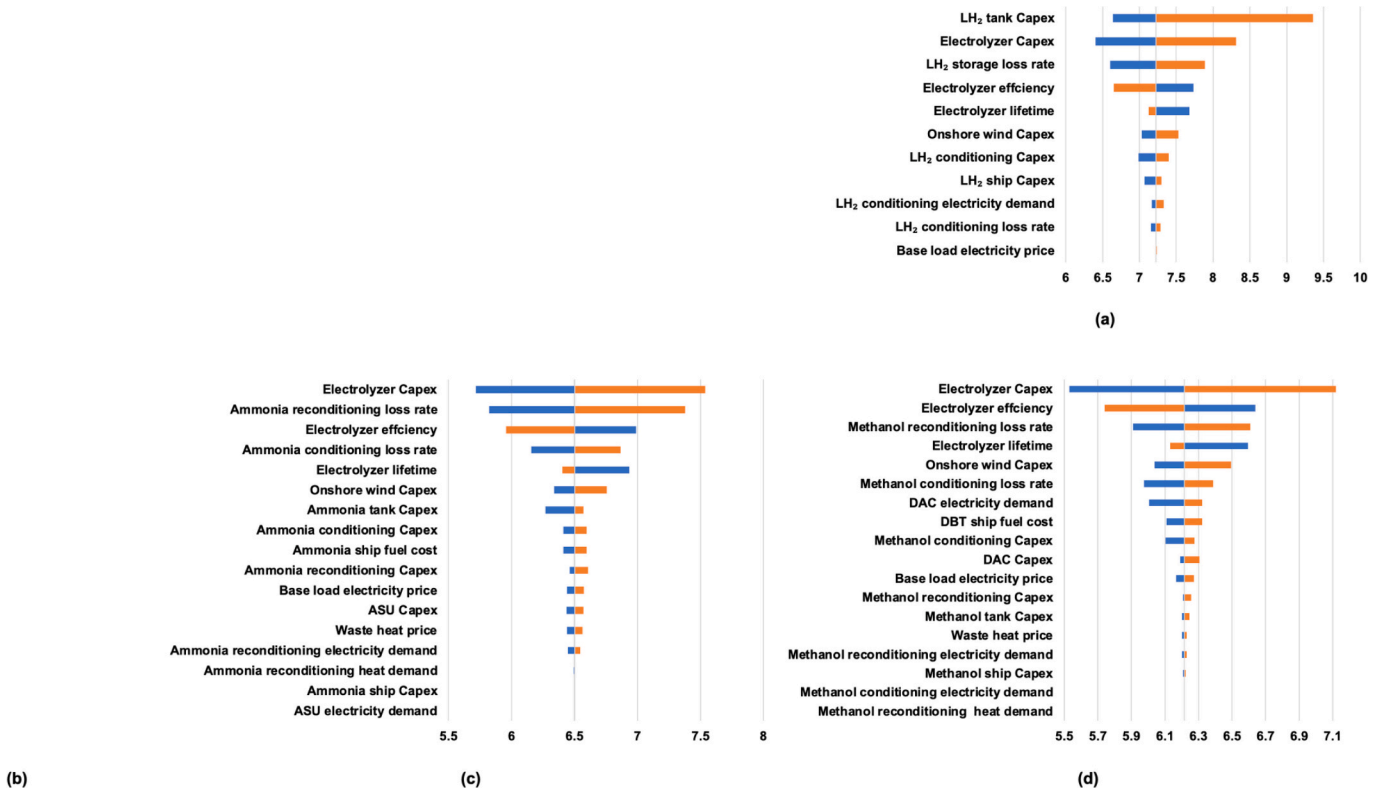

Fig. A9. Sensitivity of the LCOH ($€_{2020}/kg_{H2}$) to the input parameters of the chains belonging to the overseas-wind group. (a) the LH_2 chain, (b) the LOHC chain, (c) the NH_3 chain, (d) the CH_3OH chain.

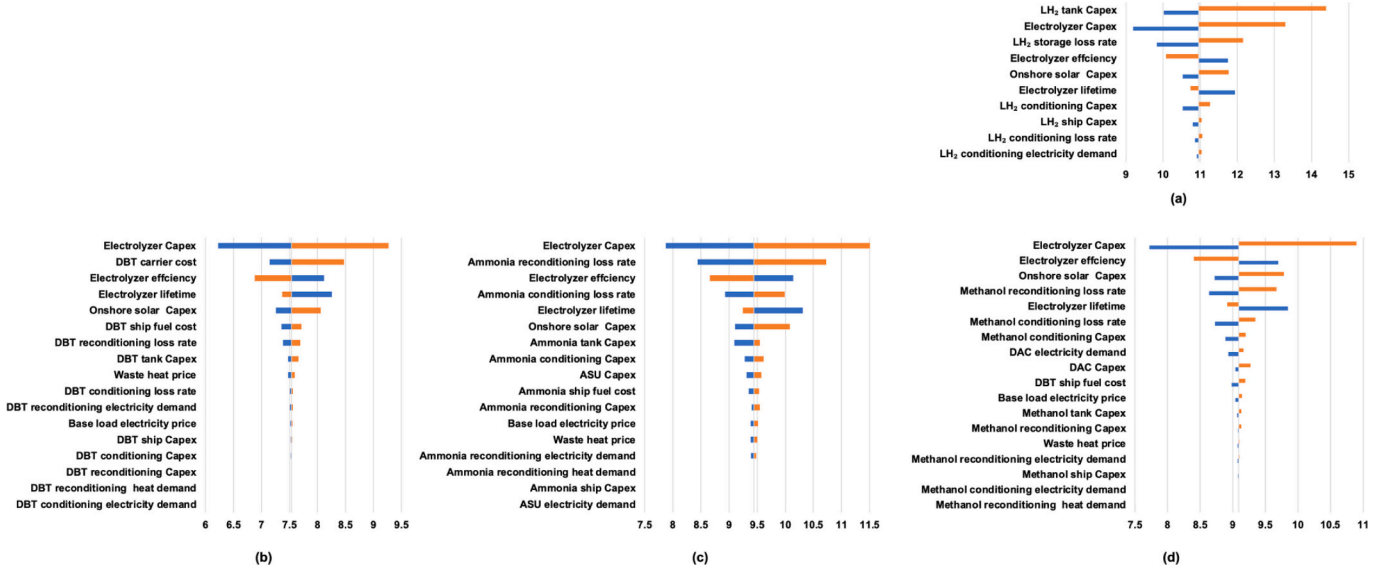

Fig. A10. Sensitivity of the LCOH ($€_{2020}/kg_{H2}$) to the input parameters of the chains belonging to the overseas-solar group. (a) the LH_2 chain, (b) the LOHC chain, (c) the NH_3 chain, (d) the CH_3OH chain.

Data availability

Data will be made available on request.

References

[1] Ren M, Lu P, Liu X, Hossain MS, Fang Y, Hanaoka T, et al. Decarbonizing China's iron and steel industry from the supply and demand sides for carbon neutrality. Appl Energy 2021;298.
[2] Fan Z, Friedmann SJ. Low-carbon production of iron and steel: technology options, economic assessment, and policy. Joule 2021;5:829–62.
[3] WSA. Sustainable steel. 2021.
[4] IEA. Iron and Steel Technology Roadmap. 2021.
[5] Jacobasch E, Herz G, Rix C, Müller N, Reichelt E, Jahn M, et al. Economic evaluation of low-carbon steelmaking via coupling of electrolysis and direct reduction. J Clean Prod 2021;328.
[6] Zhang X, Jiao K, Zhang J, Guo Z. A review on low carbon emissions projects of steel industry in the world. J Clean Prod 2021;306.
[7] Pimm AJ, Cockerill TT, Gale WF. Energy system requirements of fossil-free steelmaking using hydrogen direct reduction. J Clean Prod 2021;312.
[8] Weigel M, Fischedick M, Marzinkowski J, Winzer P. Multicriteria analysis of primary steelmaking technologies. J Clean Prod 2016;112:1064–76.

[9] Fischedick M, Marzinkowski J, Winzer P, Weigel M. Techno-economic evaluation of innovative steel production technologies. J Clean Prod 2014;84:563–80.
[10] LeadIT. Green Steel Tracker. 2023.
[11] Vogl V, Åhman M, Nilsson LJ. Assessment of hydrogen direct reduction for fossil-free steelmaking. J Clean Prod 2018;203:736–45.
[12] Somers J. Technologies to decarbonise the EU steel industry. 2022.
[13] Li F, Chu M, Tang J, Liu Z, Zhao Z, Liu P, et al. Quantifying the energy saving potential and environmental benefit of hydrogen-based steelmaking process: status and future prospect. Appl Therm Eng 2022;211:118489.
[14] Elsheikh H, Eveloy V. Assessment of variable solar-and grid electricity-driven power-to-hydrogen integration with direct iron ore reduction for low-carbon steel making. Fuel 2022;324:124758.
[15] Superchi F, Mati A, Carcasci C, Bianchini A. Techno-economic analysis of wind-powered green hydrogen production to facilitate the decarbonization of hard-to-abate sectors: a case study on steelmaking. Appl Energy 2023;342:121198.
[16] Devlin A, Yang A. Regional supply chains for decarbonising steel: energy efficiency and green premium mitigation. Energy Convers Manag 2022;254:115268.
[17] Ortiz Cebolla R, Dolci F, Weidner E. Assessment of Hydrogen Delivery Options Publications Office of the European Union. 2022.
[18] Miao B, Giordano L, Chan SH. Long-distance renewable hydrogen transmission via cables and pipelines. Int J Hydrog Energy 2021;46:18699–718.
[19] IRENA. Renewable power generation costs in 2021. 2021.
[20] Song P, Sui Y, Shan T, Hou J, Wang X. Assessment of hydrogen supply solutions for hydrogen fueling station: a Shanghai case study. Int J Hydrog Energy 2020;45:32884–98.
[21] Sens L, Neuling U, Wilbrand K, Kaltschmitt M. Conditioned hydrogen for a green hydrogen supply for heavy duty-vehicles in 2030 and 2050–a techno-economic well-to-tank assessment of various supply chains. Int J Hydrog Energy 2024;52:1185–207.
[22] Niermann M, Drünert S, Kaltschmitt M, Bonhoff K. Liquid organic hydrogen carriers (LOHCs) – techno-economic analysis of LOHCs in a defined process chain. Energy Environ Sci 2019;12:290–307.
[23] Hong X, Thaore VB, Karimi IA, Farooq S, Wang X, Usadi AK, et al. Techno-enviro-economic analyses of hydrogen supply chains with an ASEAN case study. Int J Hydrog Energy 2021;46:32914–28.
[24] Li L, Aravind PV, Woudstra T, van den Broek M. Assessing the waste heat recovery potential of liquid organic hydrogen carrier chains. Energy Convers Manag 2023;276:116555.
[25] Niermann M, Drünert S, Kaltschmitt M, Bonhoff K. Liquid organic hydrogen carriers (LOHCs)–techno-economic analysis of LOHCs in a defined process chain. Energy Environ Sci 2019;12:290–307.
[26] Statista. Europäische Union[1] & Eurozone[2]: Inflationsrate von 2001 bis 2022. 2023.
[27] Macrotrends. Euro Dollar Exchange Rate (EUR USD) - Historical Chart. 2023.
[28] Sens L, Neuling U, Wilbrand K, Kaltschmitt M. Conditioned hydrogen for a green hydrogen supply for heavy duty-vehicles in 2030 and 2050–a techno-economic well-to-tank assessment of various supply chains. Int J Hydrog Energy 2024;52:1185–207.
[29] Brändle G, Schönfisch M, Schulte S. Estimating long-term global supply costs for low-carbon hydrogen. Appl Energy 2021;302:117481.
[30] Krishnan S, Koning V, de Groot MT, de Groot A, Mendoza PG, Junginger M, et al. Present and future cost of alkaline and PEM electrolyser stacks. Int J Hydrog Energy 2023;48:32313–30.
[31] Sens L, Neuling U, Kaltschmitt M. Capital expenditure and levelized cost of electricity of photovoltaic plants and wind turbines–development by 2050. Renew Energy 2022;185:525–37.
[32] Schmidt O, Gambhir A, Staffell I, Hawkes A, Nelson J, Few S. Future cost and performance of water electrolysis: an expert elicitation study. Int J Hydrog Energy 2017;42:30470–92.
[33] Fasihi M, Breyer C. Baseload electricity and hydrogen supply based on hybrid PV-wind power plants. J Clean Prod 2020;243:118466.
[34] Caldera U, Bogdanov D, Breyer C. Local cost of seawater RO desalination based on solar PV and wind energy: a global estimate. Desalination 2016;385:207–16.
[35] Caldera U, Breyer C. Learning curve for seawater reverse osmosis desalination plants: capital cost trend of the past, present, and future. Water Resour Res 2017;53:10523–38.
[36] Reuß M, Grube T, Robinius M, Preuster P, Wasserscheid P, Stolten D. Seasonal storage and alternative carriers: a flexible hydrogen supply chain model. Appl Energy 2017;200:290–302.
[37] Yousefi SH, Groenenberg R, Koornneef J, Juez-Larré J, Shahi M. Techno-economic analysis of developing an underground hydrogen storage facility in depleted gas field: a Dutch case study. Int J Hydrog Energy 2023;48:28824–42.
[38] van Gerwen R, Eijgelaar M, Bosma T. Hydrogen in the electricity value chain. 2019.
[39] Niermann M, Timmerberg S, Drünert S, Kaltschmitt M. Liquid organic hydrogen carriers and alternatives for international transport of renewable hydrogen. Renew Sust Energ Rev 2021;135.
[40] Talukdar M, Blum P, Heinemann N, Miocic J. Techno-economic analysis of underground hydrogen storage in Europe, Available at SSRN 4524439. 2023.
[41] Lee J-S, Cherif A, Yoon H-J, Seo S-K, Bae J-E, Shin H-J, et al. Large-scale overseas transportation of hydrogen: comparative techno-economic and environmental investigation. Renew Sust Energ Rev 2022;165:112556.
[42] Campion N, Nami H, Swisher PR, Hendriksen PV, Münster M. Techno-economic assessment of green ammonia production with different wind and solar potentials. Renew Sust Energ Rev 2023;173:113057.
[43] Ikäheimo J, Kiviluoma J, Weiss R, Holttinen H. Power-to-ammonia in future north European 100% renewable power and heat system. Int J Hydrog Energy 2018;43:17295–308.
[44] Baldi F, Coraddu A, Kalikatzarakis M, Jeleňová D, Collu M, Race J, et al. Optimisation-based system designs for deep offshore wind farms including power to gas technologies. Appl Energy 2022;310:118540.
[45] Giampieri A, Ling-Chin J, Roskilly AP. Techno-economic assessment of offshore wind-to-hydrogen scenarios: a UK case study. Int J Hydrog Energy 2023;52:589–617.
[46] Giddey S, Badwal S, Munnings C, Dolan M. Ammonia as a renewable energy transportation media. ACS Sustain Chem Eng 2017;5:10231–9.
[47] Hall W, Millner R, Rothberger J, Singh A, Shah C. Green steel through hydrogen direct reduction: A study on the role of hydrogen in the Indian iron and steel sector. New Delhi: The Energy and Resources Institute (TERI); 2021.
[48] Fasihi M, Efimova O, Breyer C. Techno-economic assessment of CO2 direct air capture plants. J Clean Prod 2019;224:957–80.
[49] Niermann M, Timmerberg S, Drünert S, Kaltschmitt M. Liquid organic hydrogen carriers and alternatives for international transport of renewable hydrogen. Renew Sust Energ Rev 2021;135:110171.
[50] Franco BA, Baptista P, Neto RC, Ganilha S. Assessment of offloading pathways for wind-powered offshore hydrogen production: energy and economic analysis. Appl Energy 2021;286:116553.
[51] Stolz B, Held M, Georges G, Boulouchos K. Techno-economic analysis of renewable fuels for ships carrying bulk cargo in Europe, nature. Energy 2022;7:203–12.
[52] Gu Y, Chen Q, Xue J, Tang Z, Sun Y, Wu Q. Comparative techno-economic study of solar energy integrated hydrogen supply pathways for hydrogen refueling stations in China. Energy Convers Manag 2020;223:113240.
[53] Jouhara H, Khordehgah N, Almahmoud S, Delpech B, Chauhan A, Tassou SA. Waste heat recovery technologies and applications. Thermal Sci Eng Progress 2018;6:268–89.
[54] Wang RQ, Jiang L, Wang YD, Roskilly AP. Energy saving technologies and mass-thermal network optimization for decarbonized iron and steel industry: a review. J Clean Prod 2020;274.
[55] Keplinger T, Haider M, Steinparzer T, Patrejko A, Trunner P, Haselgrübler M. Dynamic simulation of an electric arc furnace waste heat recovery system for steam production. Appl Therm Eng 2018;135:188–96.
[56] Krüger A, Andersson J, Grönkvist S, Cornell A. Integration of water electrolysis for fossil-free steel production. Int J Hydrog Energy 2020;45:29966–77.
[57] Müller N, Herz G, Reichelt E, Jahn M, Michaelis A. Assessment of fossil-free steelmaking based on direct reduction applying high-temperature electrolysis. Cleaner Eng Technol 2021;4.
[58] Lee S, Kim T, Han G, Kang S, Yoo Y-S, Jeon S-Y, et al. Comparative energetic studies on liquid organic hydrogen carrier: a net energy analysis. Renew Sust Energ Rev 2021;150.
[59] Wang H, Zhou X, Ouyang M. Efficiency analysis of novel liquid organic hydrogen carrier technology and comparison with high pressure storage pathway. Int J Hydrog Energy 2016;41:18062–71.
[60] Obara SY. Energy and exergy flows of a hydrogen supply chain with truck transportation of ammonia or methyl cyclohexane. Energy 2019;174:848–60.
[61] Hurskainen M, Ihonen J. Techno-economic feasibility of road transport of hydrogen using liquid organic hydrogen carriers. Int J Hydrog Energy 2020;45:32098–112.
[62] RenewablesNow. BASF forges ahead with 54-MW green hydrogen project. 2023.
[63] AirLiquide. Air Liquide takes a further step in developing the hydrogen sector in France. 2023.